Precambrian Research 224 (2013) 551–569

Contents lists available at SciVerse ScienceDirect

Precambrian Research

journal homepage: www.elsevier.com/locate/precamres

Local $\delta^{34}S$ variability in ~580 Ma carbonates of northwestern Mexico and the Neoproterozoic marine sulfate reservoir

Sean J. Loyd[a,*], Pedro J. Marenco[c], James W. Hagadorn[d], Timothy W. Lyons[e], Alan J. Kaufman[f], Francisco Sour-Tovar[g], Frank A. Corsetti[b]

[a] Department of Earth and Space Sciences, University of California, Los Angeles, 595 Charles Young Drive East, Los Angeles, CA 90095, USA
[b] Department of Earth Sciences, University of Southern California, 3651 Trousdale Avenue, Los Angeles, CA 90089, USA
[c] Department of Geology, Bryn Mawr College, 101 N. Merion Avenue, Bryn Mawr, PA 19010, USA
[d] Denver Museum of Nature and Science, 2001 Colorado Boulevard, Denver, CO 80205, USA
[e] Department of Earth Sciences, University of California, Riverside, CA 92521, USA
[f] Department of Geology and ESSIC, University of Maryland, College Park, MD 20742, USA
[g] Museo de Paleontología, Departamento de Biología Evolutiva, Facultad de Ciencias, Universidad Nacional Autónoma de México, Ciudad Universitaria, México, DF, Mexico

ARTICLE INFO

Article history:
Received 9 January 2012
Received in revised form
29 September 2012
Accepted 10 October 2012
Available online 2 November 2012

Keywords:
Sulfur isotopes
Carbon isotopes
Neoproterozoic
Oxygenation
Sulfate
Diagenesis

ABSTRACT

Many $\delta^{34}S$ records have been produced from carbonate-associated sulfate (CAS) in order to understand the oxidation state of the Neoproterozoic oceans, but interregional correlation is complicated by the absence of robust chronostratigraphic markers. Here, a globally correlatable stratigraphic interval containing the Wonoka–Shuram (W–S) $\delta^{13}C$ excursion was analyzed to explore variability in the sulfur isotope record. In the excursion-containing units, the local $\delta^{34}S$ record from multiple, closely spaced sections in Sonora, Mexico, was examined to explore potential heterogeneities, and then these were compared to more distant sections elsewhere.

In Sonora, the inception and isotopic minimum of the W–S excursion is located in the Clemente Formation and coincides with an extensive oolite marker bed. Five sections containing this marker bed span ~25 km of lateral distance, exhibit significant variability in $\delta^{34}S_{CAS}$ (range: +18.6 to +27.6‰ VCDT) and high variability in CAS concentration (range: <30 to >1200 ppm). Unlike the $\delta^{34}S_{CAS}$ values, CAS concentrations show strong negative correlation with Mn/Sr ratios and Fe_{carb} concentrations, consistent with CAS removal upon diagenetic recrystallization and an absence of an accompanying sulfur isotopic fractionation. Indeed, samples containing low CAS concentrations exhibit petrographic characteristics consistent with diagenetic recrystallization including fabric destructive neomorphism and relatively coarse-crystalline textures.

Coeval W–S strata in Death Valley, Oman and the least altered Sonora samples record a decrease in $\delta^{34}S_{CAS}$ and an increase in CAS concentration; however, the magnitude of the changes are distinct, perhaps reflecting differential response to a transient oxidation event. In contrast, time equivalent facies of South China do not exhibit a decrease in $\delta^{34}S_{CAS}$ nor a relative increase in CAS concentrations. The variability in geochemical characteristics likely developed from local and/or regional marine $\delta^{34}S_{sulfate}$ heterogeneity.

Although Neoproterozoic oceanic heterogeneity in $\delta^{34}S_{sulfate}$ has been proposed, it has not been reported on such close spatial scales. In addition, the existence of variability among the Sonora sections in which strata were all deposited at similar depth indicates that heterogeneity could have occurred laterally. Finally, these findings demonstrate that while CAS concentrations may be drastically affected by diagenesis, $\delta^{34}S_{CAS}$ may retain primary signatures.

1. Introduction

Stable isotopic compositions ($\delta^{13}C$ and $\delta^{34}S$) of Neoproterozoic and Cambrian marine precipitates (i.e., limestones, dolostones and evaporites) display extreme stratigraphic trends (Fike et al., 2006; Gill et al., 2011; Halverson et al., 2005 and references therein; Hurtgen et al., 2004, 2005, 2009; Kaufman et al., 2007; Li et al., 2010; Loyd et al., 2012; McFadden et al., 2008; Xiao et al., 2012). The similarity in $\delta^{13}C_{carb}$ values (the carbon isotope compositions of carbonates) among temporally equivalent rock units has prompted the use of carbon isotope chemostratigraphy as a correlation tool in the absence of biostratigraphic and radiometric constraints (Halverson et al., 2005). Unlike what is generally accepted for $\delta^{13}C_{carb}$, the $\delta^{34}S_{sulfate}$ of evaporites and trace sulfate

* Corresponding author. Tel.: +1 949 338 2461.
E-mail address: seanloyd@ess.ucla.edu (S.J. Loyd).

0301-9268/$ – see front matter © 2012 Elsevier B.V. All rights reserved.
http://dx.doi.org/10.1016/j.precamres.2012.10.007

(carbonate-associated sulfate: CAS) in carbonate rocks have not been shown to be globally homogeneous, and yet many Neoproterozoic studies suggest that single basin trends in both $\delta^{13}C_{carb}$ and $\delta^{34}S_{sulfate}$ are related to global phenomena (cf., Fike et al., 2006; Fike and Grotzinger, 2008; Halverson et al., 2012; Halverson and Hurtgen, 2007; Hurtgen et al., 2005; Kaufman et al., 2007; McFadden et al., 2008). In more recent years, the hypothesis of a Neoproterozoic ocean with heterogeneous $\delta^{34}S_{sulfate}$ has gained support (see Lyons et al., 2012). Two styles of heterogeneity have been proposed, including vertical ocean stratification (or 'depth heterogeneity', Li et al., 2010; Shen et al., 2008, 2010, 2011; Xiao et al., 2012) and lateral variability ('horizontal heterogeneity', Hurtgen et al., 2006; Loyd et al., 2012; Lyons and Gill, 2008; Lyons et al., 2009, 2012). Indeed, lateral variability seems apparent when all of the available Neoproterozoic data are considered together, with the implicit assumption that the successions have not been altered through diagenesis. In order to better understand the Neoproterozoic ocean system, it is necessary to evaluate the extent of lateral sulfur isotope heterogeneity and determine if closely spaced, depth-equivalent stratigraphic sections record similar $\delta^{34}S_{CAS}$ signatures.

The most distinctive carbon isotopic event in Neoproterozoic time (and perhaps all time), is the so-called Wonoka–Shuram excursion (W–S), wherein carbonate $\delta^{13}C$ values plummet to ~−11‰ at ~580 million years ago (Ma; the purported age of an immediately underlying unconformity in Oman; Bowring et al., 2002) and exhibit a subsequent period of protracted carbon isotope recovery to values near 0‰ (e.g., Le Guerroue et al., 2006a). Whether a primary or secondary feature, the W–S provides a unique tie point, as it has been identified in many successions around the world, including Oman, Namibia, Australia, India, Brazil, Argentina, South China, eastern China, the southwestern United States and northwestern Mexico (Amthor et al., 2003; Bowring et al., 2007; Burns and Matter, 1993; Burns et al., 1994; Calver, 2000; Canfield et al., 2007; Condon et al., 2005; Corsetti and Kaufman, 2003; Fike et al., 2006; Gomez Peral et al., 2007; Grotzinger et al., 2011; Halverson et al., 2005; Jiang et al., 2007; Kaufman et al., 2006, 2007; Le Guerroue et al., 2006a,b; Loyd et al., 2012; Macdonald et al., 2009; McFadden et al., 2008; Nascimento et al., 2007; Nogueira et al., 2007; Prave et al., 2009; Sperling et al., 2007; Zhou and Xiao, 2007). Some authors have attributed the W–S event to either meteoric (Knauth and Kennedy, 2009; Swart and Kennedy, 2012) or burial diagenesis (Derry, 2010). However, the ubiquity of the excursion among multiple basins confirms its retained utility as a stratigraphic marker, regardless of its origin (see recent synopsis by Grotzinger et al. (2011)). Here, the W–S excursion is used as a synchronous stratigraphic tie-point to allow comparison of the $\delta^{34}S_{CAS}$ record locally, regionally and globally in order to better understand the nature of the sulfur cycle in Neoproterozoic time.

Carbonates of the Clemente Formation, Sonora, Mexico, record a very large magnitude negative carbon isotope excursion (expressing values down to ~−10‰ VPDB) and have been correlated to the W–S event (Loyd et al., 2012). The excursion-containing strata are exposed as a discrete, easily traceable marker bed and extend ~25 km laterally across three mountain ranges: Cerro Rajón (CR), Cerro Clemente (CC) and Cerro Calaveras (CCv) (Fig. 1). Geochemical analyses among the three localities provide insight into the extent and variability of sulfur signatures during this time interval. Here, the lateral variability of CAS concentrations ([CAS]) and $\delta^{34}S_{CAS}$ in the marker bed are explored as well as their relationships to traditional proxies for carbonate diagenesis. The primary objectives of this study are to (1) examine the impact of diagenesis on CAS proxies (concentration and $\delta^{34}S_{CAS}$) at the local scale, (2) explore the lateral variability of [CAS] and $\delta^{34}S_{CAS}$ at ~580 Ma and (3) provide an environmental interpretation of the least altered data.

2. Geologic setting

Neoproterozoic and early Paleozoic units crop out in northwestern Sonora, Mexico, primarily to the south of the town of Caborca (Fig. 1). These strata consist of mixed siliciclastic-carbonate successions that span the late Neoproterozoic to the latest Cambrian Furongian series (Fig. 2). Dominant sedimentary lithologies include dolostone, shale and quartzite with minor chert, basalt and limestone. Miogeoclinal deposits of Cerro Rajón, the type section for Neoproterozoic units in northwestern Mexico (Stewart et al., 1984), unconformably overlie the Aibo Granite. The Aibo Granite comprises the basement rock for many of the passive margin deposits of the Sonora region and has been dated at ~1.11 Ga (Anderson et al., 1979; Rodríguez-Castañeda, 1994). Further chronological constraint is provided stratigraphically higher in the La Ciénega Formation where *Cloudina* has been reported (McMenamin, 1984, 1996; Sour-Tovar et al., 2007), representing an age of ~548 Ma (Corsetti and Hagadorn, 2000; Grotzinger et al., 1995). Within and above these *Cloudina*-bearing units, $\delta^{13}C_{carb}$ values express a short-lived negative excursion (Loyd et al., 2012), characteristic of Precambrian–Cambrian boundary sections worldwide (Corsetti and Hagadorn, 2000; Halverson et al., 2005). In agreement with a transition into Cambrian-aged rocks, *Treptichnus pedum* occurs in the lowermost member of the overlying Puerto Blanco Formation (see Fig. 2 for stratigraphic context; Sour-Tovar et al., 2007).

Approximately 200 m of massive to thinly bedded dolomite and sandy dolomite of the El Arpa and Caborca formations overlie the Aibo Granite. The contact between the El Arpa Formation and Aibo Granite is erosional and in some areas exhibits meter-scale incision. In addition, the lowermost El Arpa contains clasts of the Aibo Granite (also recognized by Anderson et al., 1979; Damon et al., 1962). The Clemente Formation occurs above the Caborca Formation at Cerro Rajón and consists of ~200 m of siliciclastic facies with minor dolomite, sandy dolomite and limestone (Stewart et al., 1984). Approximately 133 m above the Clemente–Caborca contact lies a 2.6-m-thick carbonate marker bed composed of a basal oolite and upper, finely laminated micrite (Fig. 3; discussed in detail, below). A large-magnitude negative carbon isotope excursion occurs within the marker bed, with $\delta^{13}C$ values down to ~−10‰, and is likely correlative to the ~580 Ma W–S excursion based on its magnitude and stratigraphic position (Loyd et al., 2012). Above the marker bed, the Clemente Formation returns to primarily siliciclastic strata of alternating shales and quartzites with minor thin sandy dolostone beds. The Clemente Formation is conformably overlain by the ~75 m thick fine- to medium-grained and commonly cross-bedded Pitiquito Quartzite (Stewart et al., 1984).

The aforementioned carbonate marker bed has been identified in nearly all mountain ranges of the Sonora region that host the Clemente Formation (Stewart et al., 1984). Sampled marker beds include two sections from Cerro Rajón, two from Cerro Clemente (~15 km to the south-southwest of Cerro Rajón) and one from Cerro Calaveras (~25 km to the southwest of Cerro Rajón). Strata immediately under- and overlying the marker bed at each of these localities express nearly identical lithofacies compared to the Cerro Rajón section. The strikingly similar expression of the $\delta^{13}C$ record in each of these marker beds is additional evidence for their contemporaneous deposition. Therefore, this marker bed presents an excellent opportunity for a case study to explore lateral variability over short distances in sulfur geochemical signatures during a well-defined Neoproterozoic time interval.

3. Materials and methods

Five stratigraphic sections of the carbonate marker bed were measured from three localities in the Caborca region: Cerro Rajón (CR-1 and CR-2), Cerro Clemente (CC-1 and CC-2) and Cerro

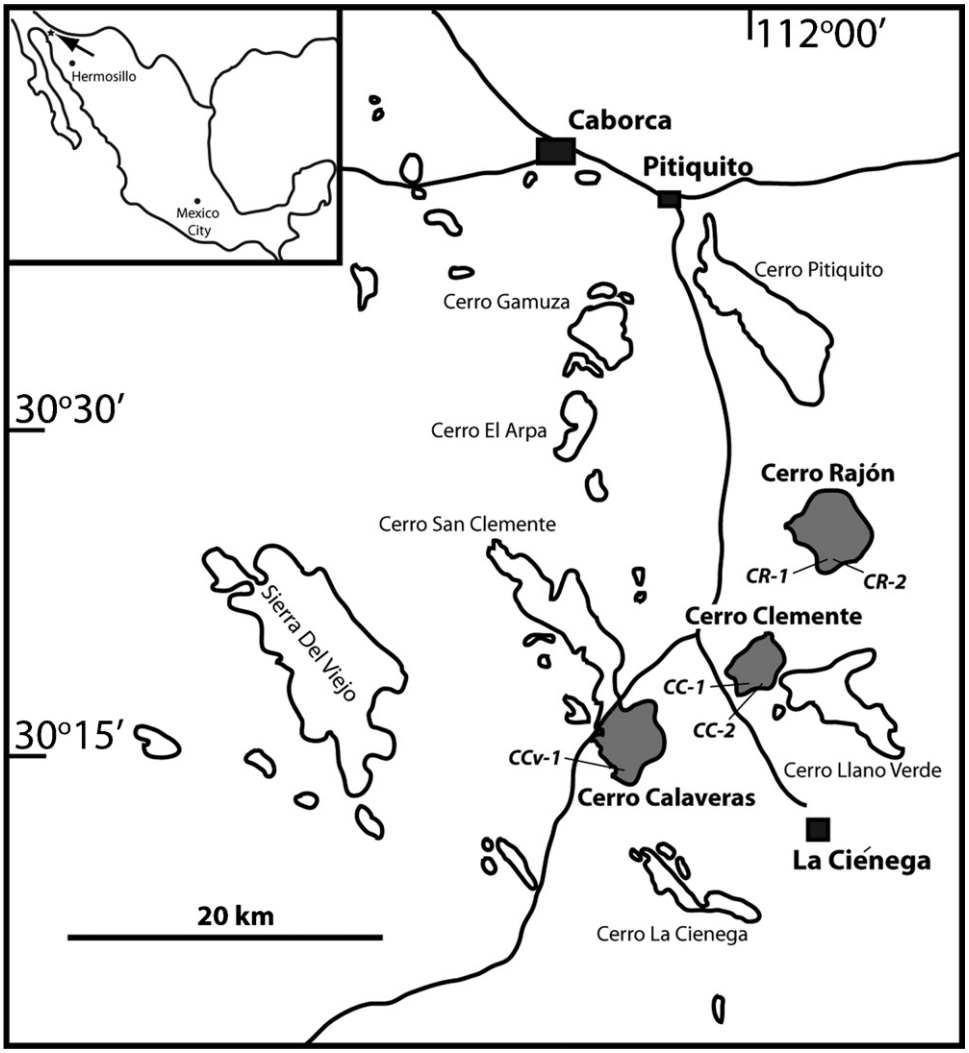

Fig. 1. Map of study sites (gray) and other Neoproterozoic facies in the Caborca region of Sonora. The approximate locations of the individual sample sites are also shown. Modified from Sour-Tovar et al. (2007).

Calaveras (CCv-1) (Fig. 1). Samples taken at regular intervals were analyzed for major and trace elemental concentration (Ca, Mg, Sr, Mn and Fe); carbonate-associated sulfate concentration; pyrite concentration and carbon, oxygen and sulfur isotope abundances ($\delta^{13}C_{carb}$, $\delta^{18}O_{carb}$, $\delta^{34}S_{CAS}$) (refer to Table 1 for geochemical data). Petrographic examination was conducted in order to confirm marker bed correlations using rare textures and structures and to document textural changes possibly associated with diagenesis.

3.1. Elemental analyses

Elemental analyses were conducted using an Agilent 7500ce ICP-MS after sample digestion in HNO_3 (2%). Ca and Mg contents are reported in weight percent (wt%), and Fe, Mn and Sr contents are reported in ppm compared to total carbonate content in each sample. Replicate analyses were better than ±30 ppm of reported values for Fe, Mn and Sr and better than ±0.5 wt% for Ca and Mg. The Ca/Mg values reported in Table 1 are molar ratios.

3.2. Carbonate-associated sulfate concentration

The CAS extraction method is modified after Burdett et al. (1989) and Marenco et al. (2008). Powdered rock samples were washed for 8–12 h four times in ultrapure (18 mΩ), de-ionized water and once in a sodium hypochlorite solution. Samples were not rinsed in NaCl solutions; however, these samples contain low pyrite concentrations and exhibit no evidence for secondary or primary sulfate minerals (anhydrite and/or gypsum) as confirmed by petrographic screening. Washed powders were acidified overnight in 3 M HCl in order to liberate lattice-bound sulfate (CAS) into solution as SO_4^{2-}. The samples were filtered down to 0.45 μm to remove insoluble residues, which were then quantified gravimetrically. The mass of the insoluble residue mass was subtracted from the initial powder mass in order to quantify weight percent carbonate (assuming that all of the dissolved material was pure carbonate). The supernatant fluids were heated to ~70 °C, and a 30% $BaCl_2$ solution was added to induce precipitation of barite. Precipitation occurred at room temperature for 72 h in order to ensure reaction completion. The precipitated barite was removed via filtration, with the resulting mass determined gravimetrically. Sulfate concentrations were calculated based on the mass of barite, and [CAS] is reported in parts per million (ppm) within the carbonate fraction in each sample by correcting for the amount of insoluble material. Duplicate measurements of [CAS] were within ±15% for individual samples.

3.3. Pyrite concentration

Pyrite concentrations were determined via the chromium reduction method described by Canfield et al. (1986). Two-gram

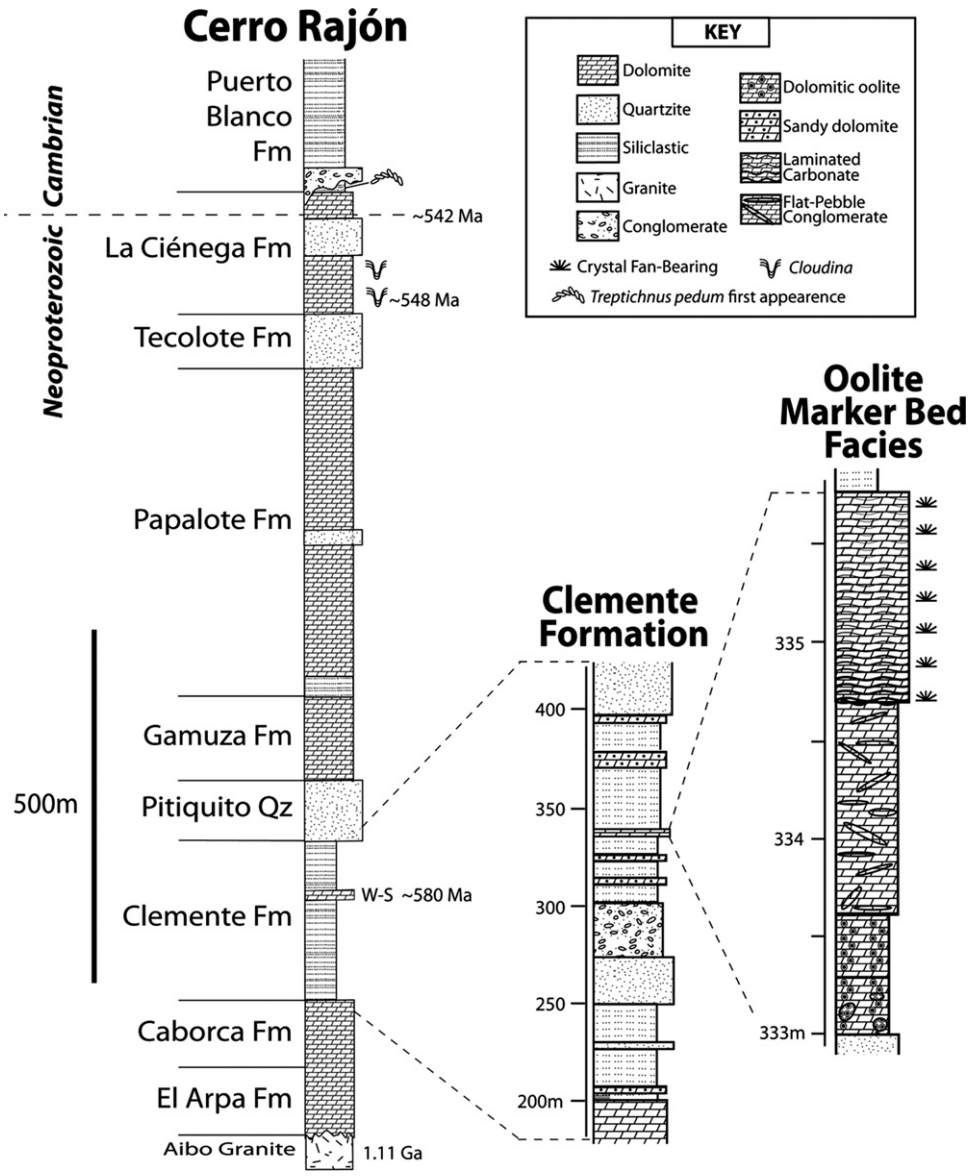

Fig. 2. Stratigraphic column of Neoproterozoic units from Cerro Rajón. Zoom-in provides stratigraphic context of marker bed facies. The marker bed exhibits carbon isotope values consistent with the ~580 Ma Wonoka–Shuram (W–S) global negative excursion. Scale bar corresponds to the left hand column. Age constraints are discussed in detail in text.

splits of the insoluble residues acquired from CAS extraction were reacted in a 1 M $CrCl_2$/HCl solution under a N_2 atmosphere. The product H_2S (gas) was passed into a trap containing a 3% $AgNO_3$/10% NH_4OH solution and captured as solid-phase Ag_2S. The precipitated silver sulfide was filtered from solution and quantified gravimetrically. Pyrite concentration was then calculated stochiometrically and reported as weight percent (wt%) compared to the original total powder mass. Replicate analyses were consistent within ±10% of the values reported here. Many replicate analyses consistently produced very low pyrite concentrations, and therefore $\delta^{34}S_{pyr}$ could not be determined.

3.4. Isotopic analyses

3.4.1. Carbon and oxygen

Carbonate carbon and oxygen isotope analyses were conducted at the University of Southern California using a VG Prism II IRMS. Samples were microdrilled from thin section billets after petrographic characterization. Replicate measurements are better than 0.1‰ for both carbon and oxygen. Oxygen and carbon isotope values are recorded in the standard δ notation in comparison to the VPDB standard.

3.4.2. Sulfur

Sulfur isotope analyses were conducted on a ThermoScientific Delta V Plus IRMS in the Laboratory of Biogeochemistry at the University of California, Riverside. The IRMS is interfaced with a Costech Analytical Technologies Inc., elemental combustion system via a Thermoscientific CONFLO III interface. Sulfur isotope values are reported in the standard δ notation in comparison to the VCDT standard. Interlaboratory comparison with the University of Maryland reveals agreement better than ±0.5‰, and replicate analyses within the individual labs yielded values consistently within ±0.1‰.

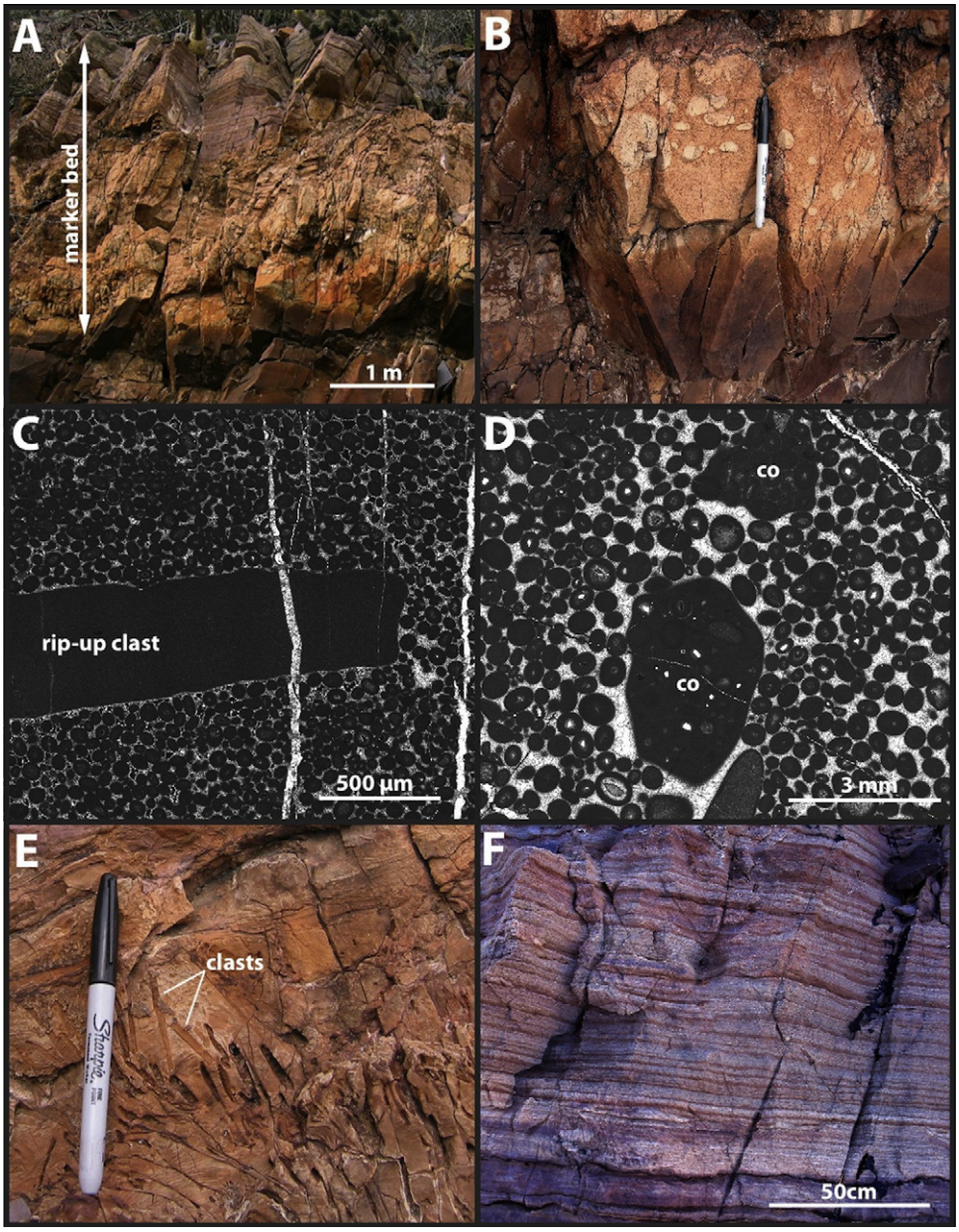

Fig. 3. Photographs of marker bed intervals. (A) Marker bed at Cerro Rajón (CR-1). (B) Close-up of lowermost oolite interval. The buff-colored clasts are composed of oolite and massive carbonate in an orange ooid matrix (pen for scale). (C) Rip-up clast within oolite interval. (D) Multiple-generation, large compound ooids (co) in oolite interval. (E) Flat-pebble conglomerate (FPC) facies (pen for scale). Notice the high variability in intraclast dips. (F) Uppermost pink and purplish laminated facies.

4. Results

4.1. Marker bed petrography

The carbonate marker bed (Fig. 3A) of the Clemente Formation exhibits a laterally consistent lithostratigraphic progression in addition to similarities in sedimentary structures, textures and microfabrics. The lowermost marker bed interval consists of basal oolite overlying reddish-brown quartzite in gradational contact (Fig. 3B–D). A buff to pinkish-gray dolostone with highly elongate intraclasts of dolomite and/or pinkish-gray limestone occurs above the oolite in most places (referred to here as flat-pebble conglomerate or FPC; Fig. 3E). A fine-scale, wavy laminated dolostone/limestone (Fig. 3F) overlies the FPC. Finally, the laminated interval is overlain by purple shale in depositional contact. At sample sites CCv-1 and CC-2, the FPC is absent, and the laminated interval is in direct contact with the underlying oolite. At CC-1, the FPC occurs between two discrete laminated horizons. Each major lithologic interval is described in detail below.

4.1.1. Oolite interval

The lowermost buff-colored oolite ranges in thickness from ~60 to 270 cm. Horizons of matrix-supported conglomerate occur within the oolite. Conglomerate clasts are typically 1–10 cm in diameter, subrounded to rounded and are composed of dolomitic oolite or buff-colored dolomite (Fig. 3B). Elongate rip-up clasts (Fig. 3C) as well as multiple-generation compound ooids (creating grains up to ~3 mm in diameter; Fig. 3D) occur within the oolite interval.

Individual ooids range in diameter from ~100 to 700 μm and are circular to oval in cross section (Figs. 4A and 5A). In well-preserved samples, ooid cortices display a radial-concentric fabric typical of

Table 1
Marker bed geochemistry.

Sample ID	Lith.	Meters above base	$\delta^{13}C_{carb}$ (‰)	$\delta^{18}O_{carb}$ (‰)	[CAS] (ppm)	$\delta^{34}S_{CAS}$ (‰)	Pyrite (wt%)	$[Sr]_{carb}$ (ppm)	$[Mn]_{carb}$ (ppm)	$[Fe]_{carb}$ (ppm)	Insol (wt%)	Mn/Sr	Mg/Ca_{mol}
CR-1													
CRCm-333	ool	0.00	−3.0	−7.5	370	+18.9	0.0130	209	973	2227	8.9	4.7	0.75
CRCm-333.15	ool	0.15	−4.4	−7.7								9.3	0.83
CRCm-333.3	ool	0.30	−5.0	−7.3								10.8	0.82
CRCm-333.45	ool	0.45	−5.5	−7.3								9.4	0.83
CRCm-333.6	FPC	0.60	−8.4	−8.5								7.0	0.85
CRCm-333.75	FPC	0.75	−9.0	−9.4								6.9	0.81
CRCm-333.9	FPC	0.90	−9.3	−10.5	36	+22.1	0.0079	121	1139	3944	20.7	9.5	0.70
CRCm-334.2	FPC	1.20	−7.9	−11.0								18.8	0.63
CRCm-334.35	FPC	1.35	−9.5	−13.4								6.0	0.05
CRCm-334.5	FPC	1.50	−8.7	−11.5								19.4	0.70
CRCm-334.6	FPC	1.60	−7.5	−10.4	287	+23.3	0.0074	110	1918	3303	18.8	17.5	0.33
CRCm-334.65	Lam	1.65	−8.9	−13.4								3.9	0.02
CRCm-334.8	Lam	1.80	−8.1	−14.1								1.8	0.02
CRCm-335.1	Lam	2.10	−8.3	−14.1								1.6	0.02
CRCm-335.35	Lam	2.35	−8.0	−13.3								0.8	0.02
CRCm-335.55	Lam	2.55	−8.7	−15.0								1.2	0.03
CRCm-335.7	Lam	2.70	−8.6	−14.9	434	+20.6	0.0000	268	815	1014	12.1	3.0	0.02
CR-2													
CO-0	ool	0.00	−5.0	−8.5	15	+23.3	0.0000	207	1161	5582	11.3	5.6	0.79
CO-30	ool	0.30	−4.8	−9.6	44	+24.9	0.0005	97	940	2556	12.4	9.7	0.78
CO-60	ool	0.60	−5.3	−7.7	279	+26.3	0.0000	80	878	1875	17.6	10.9	0.85
CO-90	FPC	0.90	−9.3	−10.5	298	+24.9	0.0000	114	1165	4571	10.4	10.2	0.72
CO-120	FPC	1.20	−8.2	−12.1	21	+18.6	0.0000	96	2250	4809	31.5	23.4	0.66
CO-150	FPC	1.50	−9.6	−12.8	17	+21.5	0.0000	143	1465	1749	15.9	10.2	0.23
CO-200	Lam	2.00	−9.2	−12.6	49	+20.1	0.0000	181	978	1435	14.6	5.4	0.10
CO-230	Lam	2.30	−8.3	−12.6	557	+23.1	0.0023	259	824	967	12.7	3.2	0.02
CO-260	Lam	2.60	−8.1	−13.4	457	+22.0	0.0021	281	1483	1204	11.1	5.3	0.03
CCv-1													
CCv-O1	ool	0.00	−4.6	−8.6	15	+26.1	0.0000	179	800	3327	14.3	4.5	0.92
CCv-O2	Lam	3.00	−8.4	−12.8	17	N/A	0.0029	134	969	1803	17.4	7.2	0.12
CCv-OL	Lam	4.00	−8.0	−11.1	28	N/A	0.0000	82	1485	4113	21.4	18.2	0.47
CC-1													
CC2-1o	ool	0.00	−3.4	−6.7	192	+27.6	0.0000	126	819	3881	8.4	6.5	0.80
CC2-2o	ool	1.50	−4.2	−6.7	291	+24.9	0.0000						
CC4	Lam	2.10	−8.1	−13.6	987	+20.1	0.0020	208	1631	449	10.7	7.8	0.02
CC5	FPC	2.70	−8.8	−14.1	466	+23.2	0.0011	199	668	564	11.8	3.4	0.04
CC6o	Lam	3.30	−7.9	−14.1	1204	+21.6	0.0000						
CC7o	Lam	4.00	−7.1	−13.1	1041	+25.5	0.0011	323	631	960	10.3	2.0	0.03
CC-2													
MX-CC-1A	ool	0.00	−5.0	−8.9	29	N/A	0.0027	149	994	4434	8.5	6.7	0.78
MX-CC-1B	ool	2.00	−5.1	−8.7	26	N/A	0.0000	121	634	2441	9.8	5.3	0.85
MX-CC-1C	Lam	4.00	−8.6	−14.5	0	N/A	0.0000	262	1160	1594	9.8	4.4	0.03

ancient ooids (e.g., Sandberg, 1975), and anhedral sparry or bladed cements fill the interstices between ooids. Where present, bladed cements exist as isopachous rims and are followed by the sparry, later-generation cement (Fig. 5A and B). Some samples do not exhibit bladed cements and are cemented entirely by blocky spar (as in Fig. 3D). Pervasive aggrading neomorphism has preferentially affected samples of CC-2 and CCv-1 versus the other localities, such that the ooids/cements are less clearly defined but still discernable (Fig. 5C).

4.1.2. Flat-pebble conglomerate interval

The middle member of the marker bed sequence is composed of buff to reddish-gray, matrix-supported, limestone/dolostone conglomerate. The intraclasts are primarily composed of reddish-gray limestone, are highly elongate and have length-to-width aspect ratios >10:1. In addition, intraclasts display a wide range of spatial orientations with inclinations between 0 and 90° compared to bedding (Fig. 3E). The matrix consists of buff-colored micrite and microspar in an interlocking mosaic. The thickness of the FPC interval is variable and ranges from being completely absent to a thickness of ~1 m. Lateral examination reveals that the FPC exhibits a lensoidal or otherwise discontinuous morphology. In rare cases, the upper laminated facies are interrupted by relatively thin intervals of FPC.

4.1.3. Laminated interval

The uppermost member of the marker bed consists of finely laminated, purple-gray to buff-gray micritic dolomite and limestone (Fig. 3F). Lamina thickness and purple coloration tend to decrease upward such that lamination is difficult to distinguish in outcrop in the uppermost centimeters. The lamination is defined by horizontal distributions of opaque inclusions or by differences in carbonate crystal size.

At study sites CR-1, CR-2 and CC-1, the laminated facies contain upwardly domed structures with fan-like morphology (Figs. 4B,C and 5D). These "fans" consist of ~100–1500 μm tall, radiating crystals with blunt terminations (Fig. 4D). In rare cases, clusters of opaque grains accumulate near the basal portions of larger crystal projections. Bedding-parallel thin sectioning exposes crystal tops with pseudohexagonal morphologies (Fig. 4E). Fans tend to occur in high abundance along particular horizons (Fig. 6), but in some cases isolated fans exist as well. In samples from

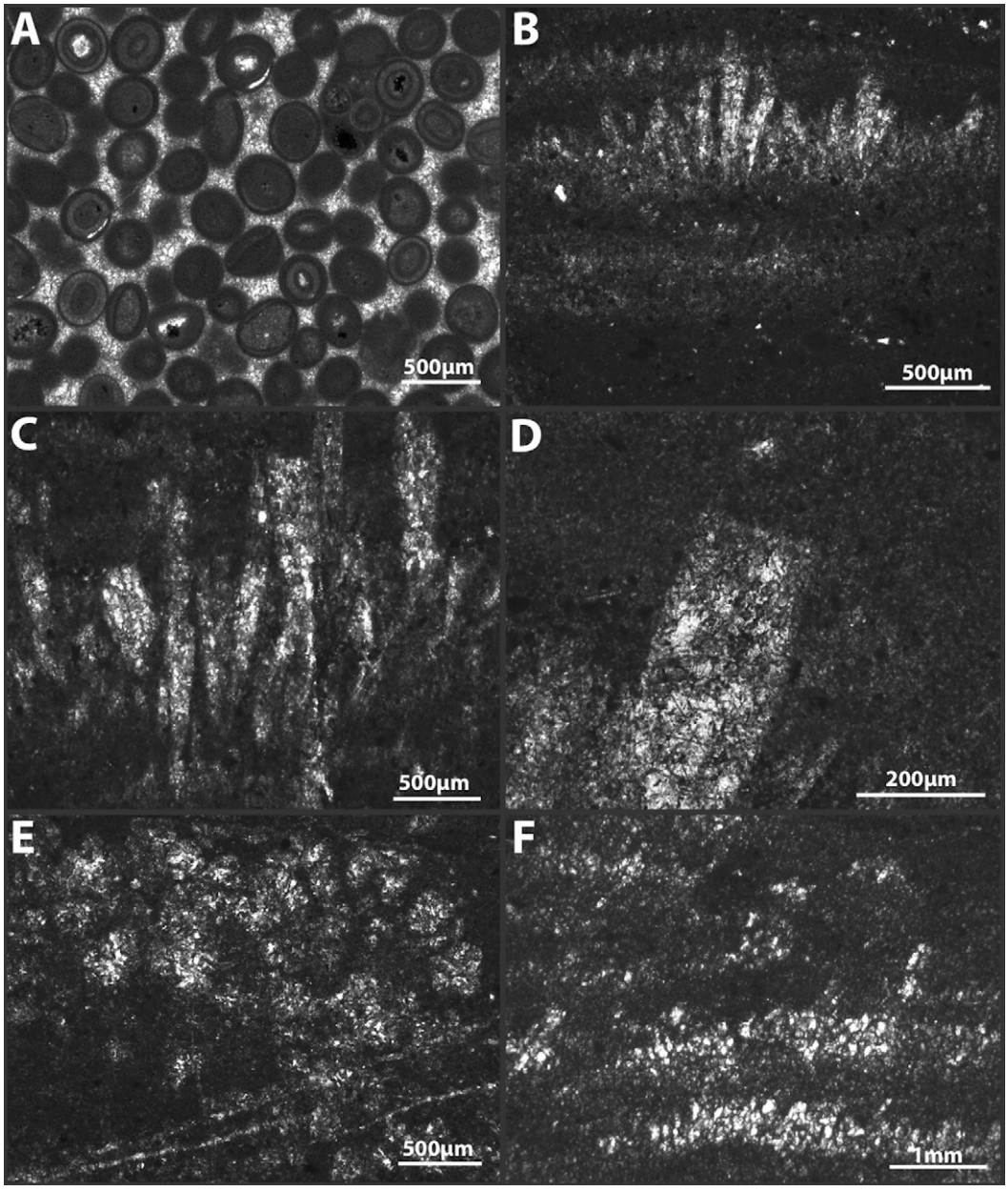

Fig. 4. Photomicrographs of oolitic and laminated intervals of the marker bed. (A) Oolite of CC-2. Interstices are filled by sparry cement. (B) Crystal fans showing radiating habit (CC-1). (C) Cluster of crystal fan blades of CR-1. (D) Close-up of fan blade from CC-1. Notice square termination, indicative of an aragonitic precursor. (E) Bedding-parallel thin section photomicrograph from laminated interval of CR-1. Notice psuedohexagonal morphology. (F) Possibly recrystallized fan grouping of CC-2. The size and upward doming shape is reminiscent of the well-preserved fans of CR-1, CR-2 and CC-1.

CC-2, clear blunt-terminating crystals are absent; however, similarly sized and shaped upward-doming features are distinguishable. These features are comparatively coarse crystalline (crystals up to 100 μm in diameter) and are more discontinuous (Figs. 4F and 5E). Samples from CCv-1 do not exhibit fans and are coarsely crystalline, and the lamination is difficult to recognize in thin section. Crystals in CCv-1 range in size from ~50 to 200 μm in diameter and are arranged in an interlocking mosaic (Fig. 5F).

4.2. Geochemistry

4.2.1. Carbon and oxygen isotopes

All five sample sites display similar trends in carbon and oxygen isotope values (Fig. 7). Oxygen isotope compositions begin at ~−8‰ (VPDB) in the basal oolite and decrease to a minimum of ~−13‰ in the uppermost laminated interval. Carbon isotopes show a similar trend, except minima typically occur near the basal or middle portions of the laminated interval. Minimum $\delta^{13}C$ values in all sections fall below −8‰ (VPDB). $\delta^{13}C_{carb}$ values from CR-1 and CR-2 include the lowest measured, with minima as low as −9.5‰. $\delta^{13}C_{carb}$ and $\delta^{18}O_{carb}$ show moderate positive correlation (Fig. 8).

4.2.2. Elemental concentration

Stratigraphic analyses of the trace elemental concentrations of Sr, Mn and Fe (referred to as Sr_{carb}, Mn_{carb} and Fe_{carb}, respectively) and major elements Ca and Mg reveal general similarities among the five sample sites (Fig. 7). Strontium concentrations

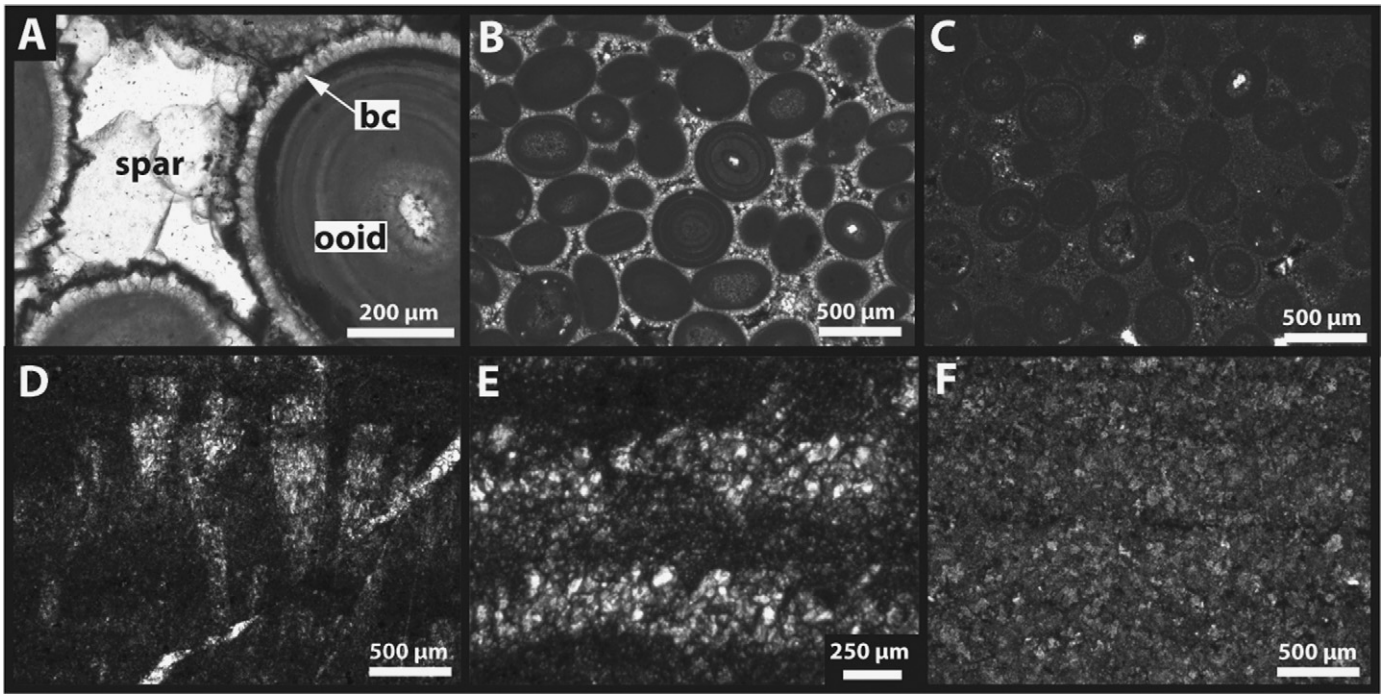

Fig. 5. Photomicrographs showing the variability in textures exhibited by the marker bed. (A) Close-up of oolite of CR-1 showing paragenetic progression from ooid (the primary depositional component), to bladed cements (bc) to sparry, pore occluding cement. Also notice well-defined ooid cortices, reflective of good preservation. (B) Ooids of CR-1 with sharp boundaries and laminae. (C) Ooids of CCv-1 with blurred boundaries and laminae. Notice ghost-like appearance. (D) Well defined fans of CR-2. (E) Doming, coarse-grained structures of CC-1. (F) Fan-free, pseudospar mosaic of the laminated member of CCv-1.

are low and range from 80 to 208 ppm in the basal oolite interval and increase to maximum concentrations between 134 and 323 ppm in the middle to uppermost portions of the laminated interval. The higher resolution sample sites (CR-1 and CR-2) show a pronounced increase in Sr_{carb} coincident with the transition into the laminated member. Sample site CCv-1 does not exhibit an increase in Sr_{carb}, and instead concentrations decrease slightly up section.

In all sections, Mn_{carb} concentrations fall between 289 and 2636 ppm. CR-1 displays elevated Mn_{carb} concentrations (between 1139 and 2636 ppm) within the FPC interval and a sharp decline (from 1918 to 982 ppm) coincident with the transition into the laminated interval. A less pronounced increase is evident at 120 cm in the FPC interval of CR-2, where Mn_{carb} concentrations reach 2250 ppm.

In general, Fe_{carb} concentrations decrease up section with the exception of CCv-1. Sample sites CR-1 and CR-2 show pronounced increases in the FPC interval. Basal Fe_{carb} concentrations are typically high (except CR-1), with values >3000 ppm and up to 5582 ppm. Concentrations are

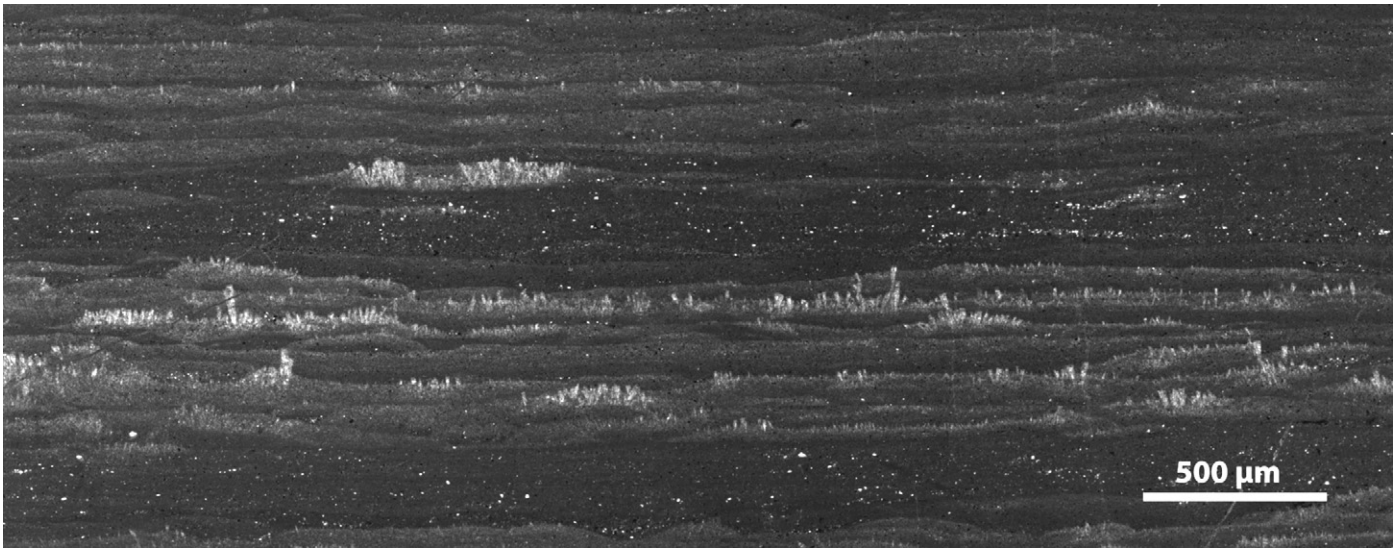

Fig. 6. Photomicrograph mosaic showing distribution of crystal fans along particular horizons.

lower in the laminated interval (with the exception of the uppermost CCv-1 data point), with values between 449 and 1594 ppm.

Aside from CCv-1, Mn/Sr ratios are relatively low in the upper laminated interval (between 0.7 and 5.4). Sample sites CR-1, CR-2 and CC-1 show a pronounced increase near the middle of the section, coincident with the FPC (CR-1 and CR-2) or lower laminated (CC-1) members. Mn/Sr values of CCv-1 increase from 4.5 in the basal oolite to 18.2 in the laminated member.

The lowermost samples of each section yield relatively high Mg/Ca (molar) ratios, approaching 1—the value of stochiometric dolomite. These values generally decrease up section, and the laminated facies exhibit ratios near zero. One exception is site CCv-1, where the uppermost data point has a Mg/Ca ratio of 0.47.

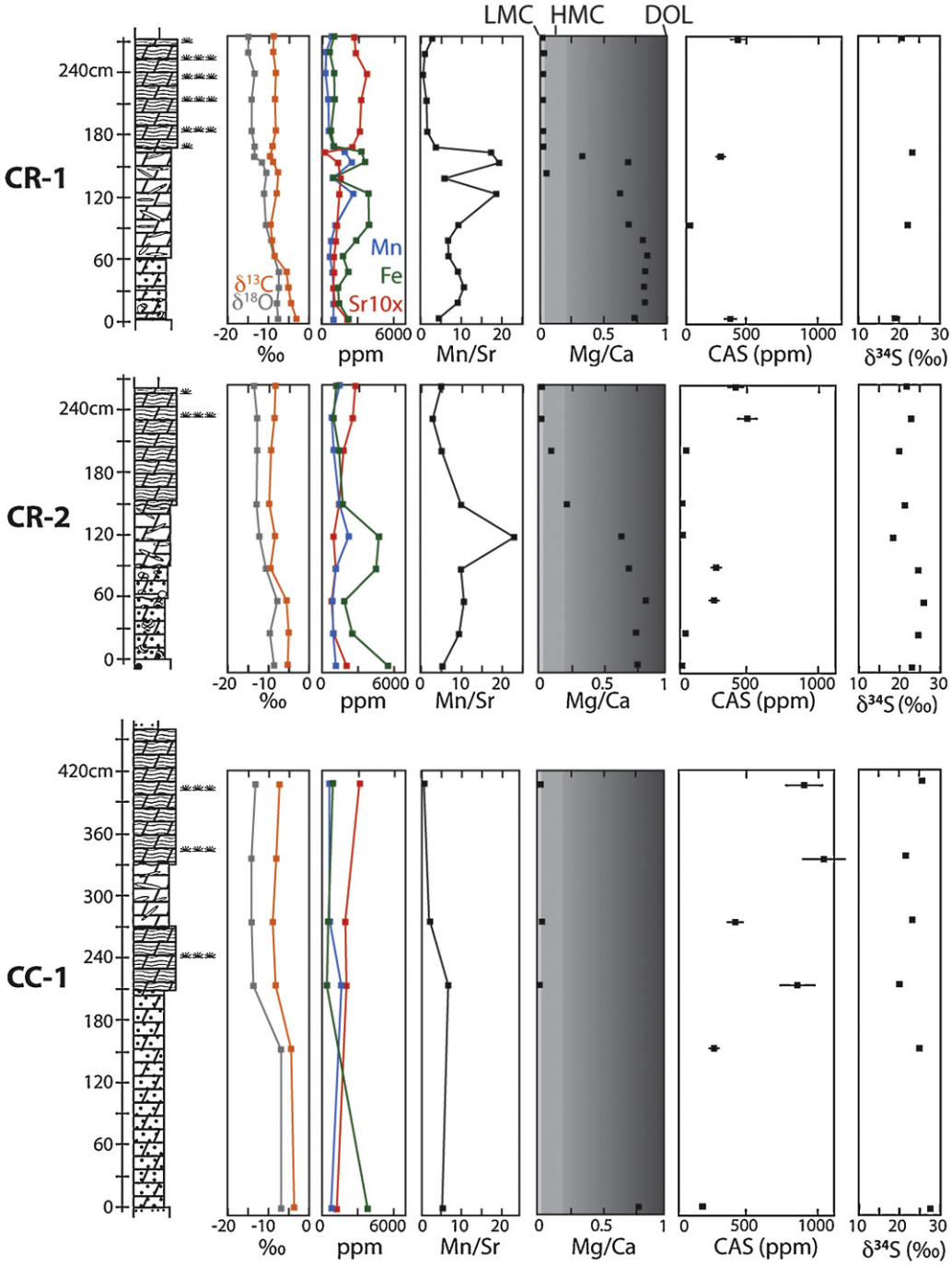

Fig. 7. Geochemical data shown stratigraphically for all five sections. Refer to Fig. 2 for stratigraphic key. Three fan icons indicate abundant crystal fans. A single fan icon indicates rare crystal fans. Fan icons with an overlying R indicate recrystallized fan horizons. Strontium concentrations are elevated 10× to enhance visualization of stratigraphic trends. Mg/Ca diagrams are separated as follows: light gray = Mg/Ca ratio consistent with low Mg calcite (LMC), gray = high Mg calcite (HMC), far right of dark gray = dolomite (DOL; Mg/Ca = 1). Notice similarity in stratigraphic trends of $\delta^{13}C_{carb}$ and $\delta^{18}O_{carb}$ and relative lack thereof in [CAS] and $\delta^{34}S_{CAS}$. The negative trend in $\delta^{13}C_{carb}$ up-section is likely the Wonoka–Shuram excursion, recognized in ~580 Ma carbonates elsewhere.

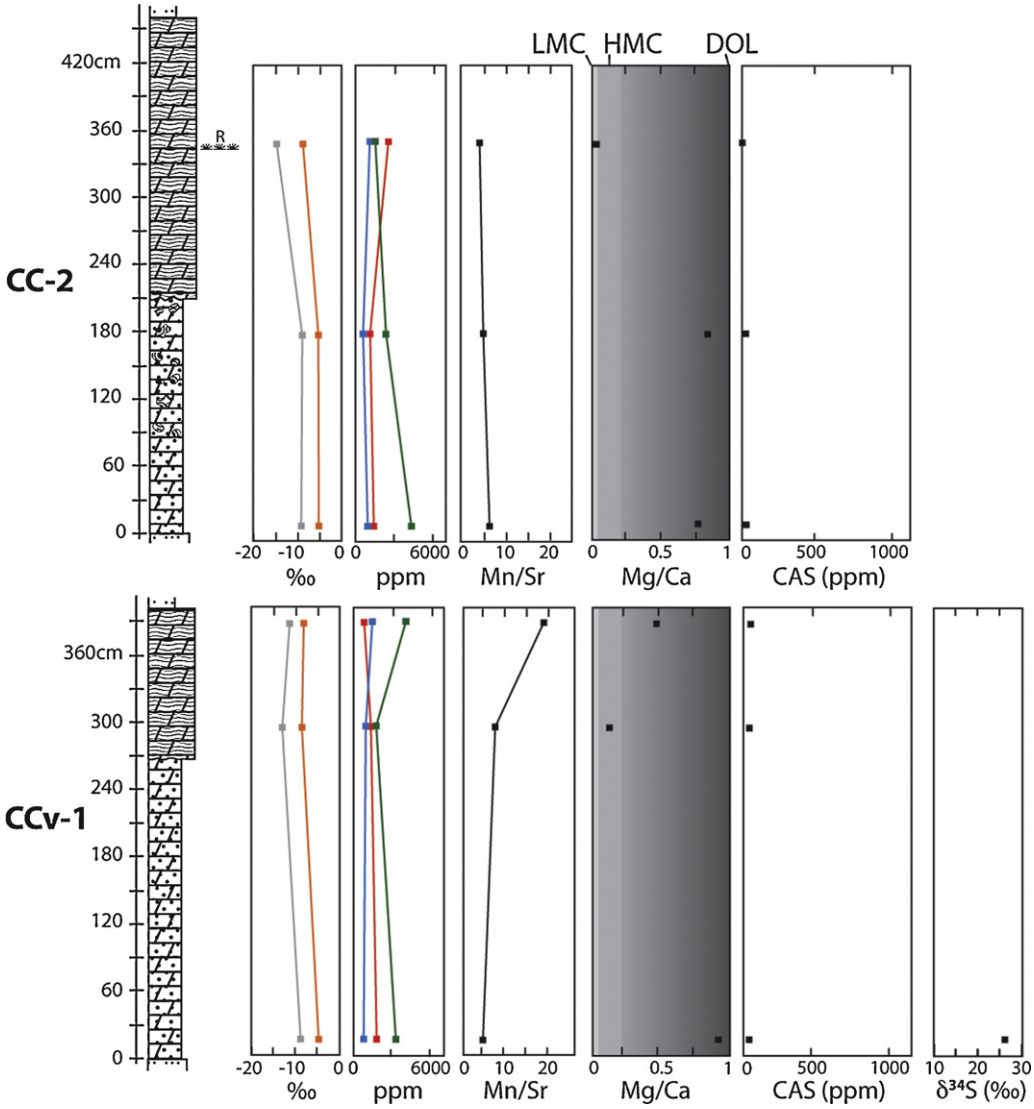

Fig. 7. (*Continued*).

4.2.3. Carbonate-associated sulfate and pyrite

CAS concentrations ([CAS]) are highly variable among the different stratigraphic sections (Figs. 7 and 9). Sites CC-2 and CCv-1 exhibit extremely low values, falling below 30 ppm. [CAS] values of CR-1 show a minimum near the basal FPC and elevated concentrations of ~400 ppm in the basal and uppermost horizons of the section. CR-2 displays high [CAS] (~500 ppm) in the upper portion of the laminated interval and uppermost oolite/lowermost FPC (~300 ppm) and low values (<49 ppm) elsewhere. CC-1 exhibits the highest [CAS], with values in excess of 1000 ppm in the laminated interval. Pyrite concentrations are low, with all samples containing less that 0.01 wt% (Supplementary Fig. 1).

Supplementary material related to this article found, in the online version, at http://dx.doi.org/10.1016/j.precamres.2012.10.007.

4.2.4. $\delta^{34}S_{CAS}$

The sulfur isotope composition of CAS varies moderately within and among the different sections studied (Figs. 7 and 9). In total, $\delta^{34}S_{CAS}$ values range from +18.6 to +27.6‰. Samples from the lower portion of the section range from +18.9 (CR-1) to +27.6‰ (CC-1), mid-section samples range from +21.5 (CR-2) to +23.3‰ (CR-1), and the upper samples range from +20.6 (CR-1) to +25.5‰ (CC-1). Sample site CC-2 lacked sufficient CAS to perform isotope analyses, and only one sample from CCv-1 yielded sufficient CAS, thus stratigraphic trends could not be developed at these sites.

5. Discussion

5.1. Marker bed depositional environment

Inter-outcrop consistencies in the succession of lithologic characteristics, as well as similar suites of depth-restricted sedimentary structures, suggest that all of the marker bed sections were deposited at similar paleo-depths. The occurrences of multiple-generation and large compound ooids, rip-up clasts and conglomeratic components within the oolite interval suggest a relatively high-energy, wave- and/or tide-influenced shallow depositional environment. Specifically, the multiple-generation, compound ooids indicate that these grains were probably not

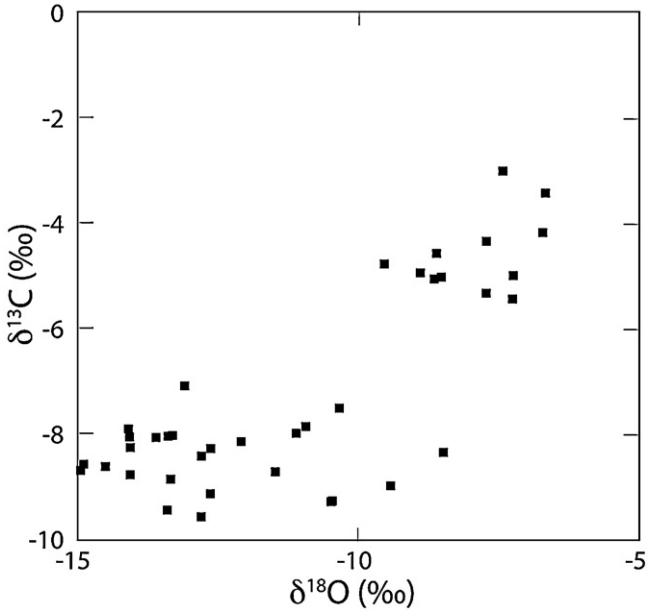

Fig. 8. Cross plot of $\delta^{13}C_{carb}$ and $\delta^{18}O_{carb}$ for all samples. Notice positive correlation.

transported significant distances from the ooid forming environment, which implies a very high energy regime with recurring resuspension of already-cemented ooids. The FPC interval is additional evidence for deposition at a very shallow depth with little post-formation clast transport (FPC's are generally interpreted as intra-formational structures).

The laminated component most likely represents a relatively deeper or more protected depositional environment. Although lamination is not depth-dependent per se, its presence together with the absence of cross-bedding, cross-lamination and channels does suggest a relatively low energy system, interpreted here as deeper than the underlying oolite and FPC.

Because this succession of sedimentologic characteristics is repeated at all of the studied sites, we can surmize that these marker beds were deposited under similar physical conditions, perhaps representing shallow oscillatory-flow-dominated paleoenvironments. Therefore, geochemical comparison among these sites may provide insight into lateral variability in ocean chemistry, provided that methodological artifacts and diagenetic alteration can be ruled-out and/or isolated (see below).

5.2. *Pyrite oxidation and the reliability of CAS in carbonates*

Marenco et al. (2008) and Mazumdar et al. (2008) demonstrated that pyrite oxidation during the CAS extraction procedure can alter the primary values of both [CAS] and $\delta^{34}S_{CAS}$. Fortunately, the low pyrite concentrations in marker bed carbonates (all samples <0.01 wt%) make alteration of this sort unlikely. Furthermore, [CAS] and $\delta^{34}S_{CAS}$ do not correlate with pyrite concentration (Supplementary Fig. 1A and B). Petrographic screening did not reveal any sulfate minerals, which would be expected to form as a result of non-methodological pyrite oxidation (in outcrop, for example). Thus, while pyrite oxidation can obscure CAS data in carbonate rocks (either during sample analysis or post-depositional alteration), it does not appear to have significantly altered those of the Clemente marker bed.

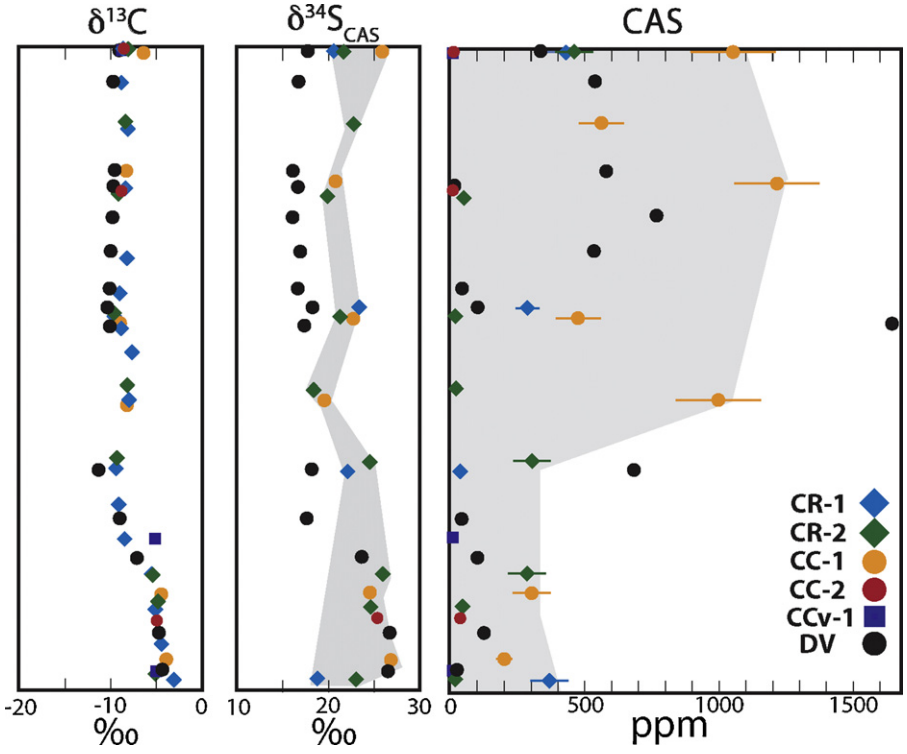

Fig. 9. Composite $\delta^{13}C_{carb}$, $\delta^{34}S_{CAS}$ and CAS concentration curves for the five Sonora study sites and those of the Rainstorm carbonates (DV). Here, sulfur curves are time-correlated via $\delta^{13}C$. Notice the moderate variability in $\delta^{34}S_{CAS}$ and high variability in CAS concentration. $\delta^{34}S_{CAS}$ and CAS concentration are significantly reduced and elevated, respectively, compared to underlying and overlying carbonates at Cerro Rajón. Gray envelopes encompass Sonora sulfur isotope and [CAS] data.

5.3. Diagenetic indicators

Although pyrite oxidation does not seem to be a major issue here, other styles of alteration during burial and their potential impacts on [CAS] and $\delta^{34}S_{CAS}$ must be considered. Sr_{carb}, Mn_{carb} and Fe_{carb} are traditionally used to assess the degree of alteration in carbonate systems due to the their relative concentrations in marine, meteoric and burial diagenetic fluids and their affinity to the carbonate crystal lattice (Bodine et al., 1965; Brand and Veizer, 1980; Kinsman, 1969; Turekian, 1972). Progressive meteoric alteration of originally marine carbonates generally leads to a decrease in Sr_{carb} and an increase in Mn_{carb} (Brand and Veizer, 1980). In addition, meteoric as well as burial diagenesis can produce decreases in both carbon and oxygen isotope compositions (Allan and Mathews, 1982; Banner and Hanson, 1990; Derry, 2010; Knauth and Kennedy, 2009; Turekian, 1972). Along with decreased $\delta^{13}C_{carb}$ and $\delta^{18}O_{carb}$ values, significant Fe_{carb} enrichments are generally attributed to recrystallization with increasing burial (e.g., Tucker and Wright, 1990).

Textural changes are also expected during progressive diagenetic alteration. In general, crystal size increases with increasing recrystallization such that the crystallographic progression should follow the trend from micrite to microspar to pseudospar in carbonates experiencing alteration (Brand and Veizer, 1980). This crystal growth has been termed aggrading neomorphism (Bathurst, 1975; Folk, 1965) and has been recognized in many carbonate systems. In addition, intricate textural features can be destroyed upon recrystallization. However, previous reports of Precambrian carbonates demonstrate that dolomitization can preserve some textures through a process known as mimetic dolomitization (Corsetti et al., 2006; Sibley, 1991; Tucker, 1983; Zempolich and Baker, 1993), wherein original sedimentary and/or crystallographic fabrics are preserved during the subsequent dolomitization.

Research by Gill et al. (2008) provided a first step toward understanding the effects of diagenesis on CAS proxies (concentrations and $\delta^{34}S_{CAS}$). In that study, the authors demonstrated that meteoric recrystallization of Pleistocene coralline aragonite to low-Mg calcite is accompanied by significant decreases in $\delta^{18}O_{carb}$, Sr_{carb}, Na_{carb} and [CAS]. In contrast, $\delta^{34}S_{CAS}$ values are relatively invariant between primary and recrystallized phases, suggesting that the sulfur isotope compositions are buffered to primary values. These findings led the authors to conclude that meteoric recrystallization can cause a reduction in [CAS] but that $\delta^{34}S_{CAS}$ is relatively unaffected and can preserve primary $\delta^{34}S_{sulfate}$ values.

5.4. Marker bed diagenesis and CAS concentration

Upon petrographic examination, it is clear that the marker beds were influenced by at least two distinct phases of diagenesis. The earlier phase corresponded to extensive oolite cementation, likely in a mixed marine–meteoric environment. This interpretation is supported by the paragenetic evolution from framework grains (ooids); followed by bladed, isopachous cements and finally blocky spar that occluded the remaining pore space (Fig. 5A and B). Such a progression is common in marine carbonates experiencing cementation during increased meteoric influence (Bathurst, 1975). The later stage(s) of diagenesis was associated with primary fabric destruction and has seemingly influenced each marker bed section to different degrees. Fig. 5B–F displays the degree of fabric destruction associated with this later period of diagenesis and its relative influence on the marker bed carbonates. The effects of late recrystallization (often described as 'increased textural maturity') are discussed further below, along with notable geochemical variability.

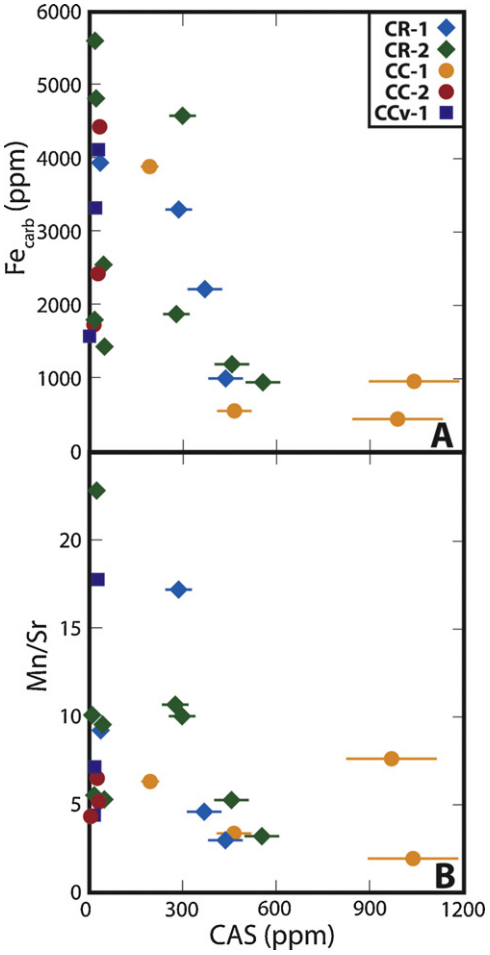

Fig. 10. Cross plots of CAS and traditional proxies of diagenesis (A) Fe_{carb} and (B) Mn/Sr. Notice how samples with high CAS correspond to decreased Fe_{carb} and Mn/Sr.

Values of [CAS] correlate inversely with Fe_{carb} and Mn/Sr (Fig. 10). These trends are consistent with meteoric and/or burial alteration of an initially marine-precipitated carbonate, as explained above. These results are in broad agreement with those of Gill et al. (2008) in that [CAS] decreases upon recrystallization.

Samples and sections exhibiting aggrading neomorphism and lacking well-defined intricate features (crystal fans, lamination and ooid cortices) exhibit low to negligible [CAS] and were likely influenced by burial diagenesis. Specifically, CC-2 and CCv-1 display [CAS] values below 30 ppm and lack well-pronounced crystal fans. CC-2 contains "fan-like" features (Figs. 4F and 5E); however, these are characterized by a coarse-crystalline, anhedral mosaic suggestive of significant aggrading neomorphism. Fan blades in CC-2 do not exhibit well-pronounced straight edges, in contrast to those of CR-1, CR-2 and CC-1, which is also indicative of recrystallization. CCv-1 contains no fans nor fan-like features and lacks a well-defined lamination (Fig. 5F). The lamination can be seen in outcrop; however, lamina transitions are obscure, and the boundaries are diffuse. In photomicrograph, the laminated facies are composed of psuedospar, likely reflecting aggrading neomorphism of a finer-grained precursor (probably micrite). In addition, the oolitic interval of CCv-1 is composed of a pseudospar mosaic, and ooids are identifiable but appear ghost-like (Fig. 5C), suggestive of recrystallization.

The above observations indicate removal of CAS during recrystallization again in agreement with the findings of Gill et al. (2008). Elevated Mn/Sr and Fe_{carb} and increased textural maturity show strong correlation with decreased [CAS]. The overall low Sr_{carb}

(140–380 ppm) and high concentrations of Mn_{carb} (290–2640 ppm) and Fe_{carb} (490–5700 ppm) are indicative of diagenetic influence in all intervals of the marker bed. Therefore, the samples with the lowest Mn/Sr ratios and Fe_{carb} and highest [CAS] are likely the best candidates for recording the primary geochemistry of coeval seawater.

It is notable that the oolite intervals of the marker beds in the most unaltered sections generally contain significantly less CAS than the corresponding laminated intervals (Fig. 7A–C). Given that the oolite interval contains a large proportion of bladed and/or blocky cements (~20% in some cases), it is likely that a large amount of carbonate was derived from a meteoric fluid (Bathurst, 1975). Since meteoric fluids contain relatively low concentrations of dissolved sulfate, it seems reasonable that the oolites would contain less CAS. As a result, the marine-dominated fan interval should be more representative of a primary marine precipitate and therefore is the primary target in our effort to reconstruct past seawater sulfate concentrations.

5.5. Diagenetic effects on $\delta^{34}S_{CAS}$

The isotopic composition of CAS is moderately variable among the sample sites. $\delta^{34}S_{CAS}$ shows no appreciable correlation with Fe_{carb}, Mn/Sr or CAS concentration (Fig. 11A–C), further supporting that diagenesis has not significantly affected the sulfur isotope composition of CAS (as proposed in Gill et al., 2008). Ultimately, the variability in $\delta^{34}S_{CAS}$ at marker bed sites may result from primary local heterogeneity in seawater $\delta^{34}S_{sulfate}$ or later, diagenetic modification during burial. Whereas diagenesis has not been conclusively identified as a $\delta^{34}S_{CAS}$ modifying process (cf., Gill et al., 2008; Lyons et al., 2004), at first glance it seems likely that diagenetic processes could preferentially affect $\delta^{34}S_{CAS}$ versus $\delta^{13}C_{carb}$, given the very high carbon content and therefore greater rock-buffering tendencies in carbonates (Banner and Hanson, 1990). However if considered further, burial diagenesis (as well as meteoric diagenesis, see Gill et al., 2008) can be ruled out as a probable modifier of the $\delta^{34}S_{CAS}$ signal, particularly if the concentration of sulfate in diagenetic fluids is considered. Although it is difficult to characterize burial diagenetic waters, it is likely that these fluids were low in sulfate (particularly if Precambrian seawater contained low sulfate and given that sulfate-rich formation waters are generally sourced from seawater) and therefore the potential for burial alteration of the $\delta^{34}S_{CAS}$ signal was probably quite limited. Thus, we prefer a primary origin of the $\delta^{34}S_{CAS}$ signal and posit that the variability observed within the oolite marker beds reflect oceanic heterogeneity in marine $\delta^{34}S_{sulfate}$.

5.6. Local seawater sulfate and $\delta^{34}S$

Although diagenetic overprinting can remove CAS, it is encouraging that samples from Neoproterozoic units retain at least some and occasionally high residual CAS. The implication is that Neoproterozoic seawater contained appreciable sulfate levels to be preserved in solid-phase carbonate. However, deriving precise sulfate concentrations in Neoproterozoic seawater (liquid concentration, mol/L) is impossible given only [CAS] in parts per million (solid concentration g/10^6 g), especially without well-known partition coefficients. Nevertheless, relative changes in concentrations of seawater sulfate using both [CAS] and $\delta^{34}S_{CAS}$ data should provide useful information. Specifically, we will compare inter-site geochemical trends for the marker bed using the $\delta^{13}C_{carb}$ record and the general lithologic intervals as correlation tie-points. The similarities in lithology and depositional depth among individual marker bed sections and intervals provide a scenario whereby geochemical variability is not likely the result of facies variability or a vertically stratified water column and therefore these sites represent an excellent case study to explore local, lateral heterogeneity.

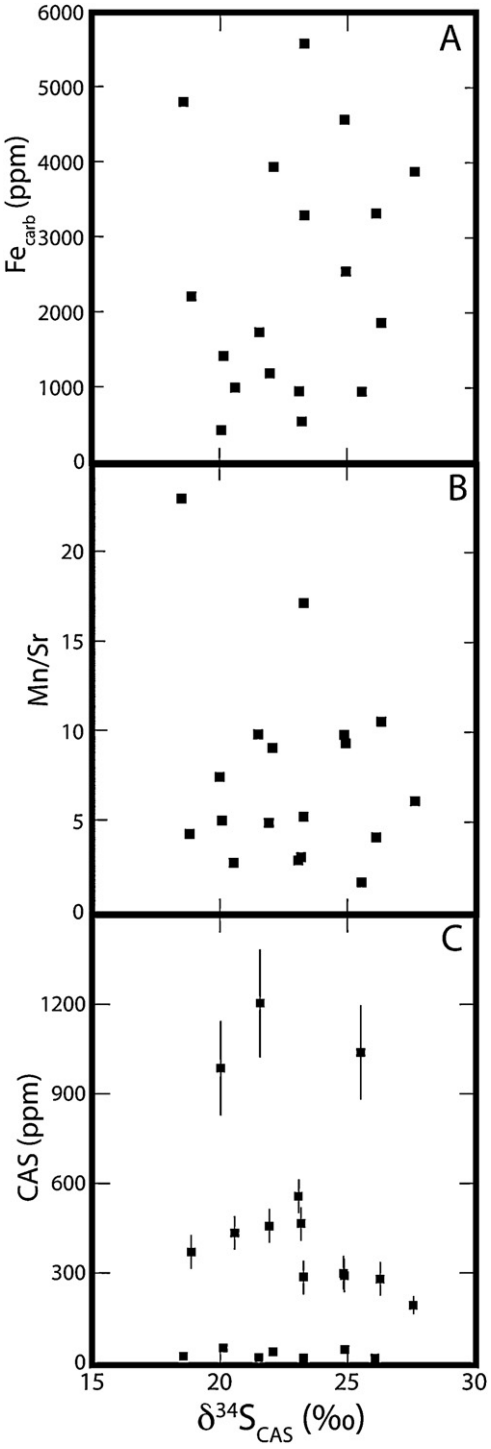

Fig. 11. Cross plots of $\delta^{34}S_{CAS}$ and traditional proxies of diagenesis (A) Fe_{carb} and (B) Mn/Sr, and (C) CAS concentration. Notice the lack of significant correlation in all three.

Values for [CAS] within the marker bed at CR-1, CR-2 and CC-1 are significantly elevated compared to units stratigraphically above and below (see Fig. 5 in Loyd et al., 2012). Non-marker bed Neoproterozoic carbonates of Cerro Rajón exhibit CAS concentrations <200 ppm (Loyd et al., 2012), in striking contrast to marker bed values of up to 1200 ppm. The increased [CAS] of the marker beds are not likely a strict consequence of a facies-dependence

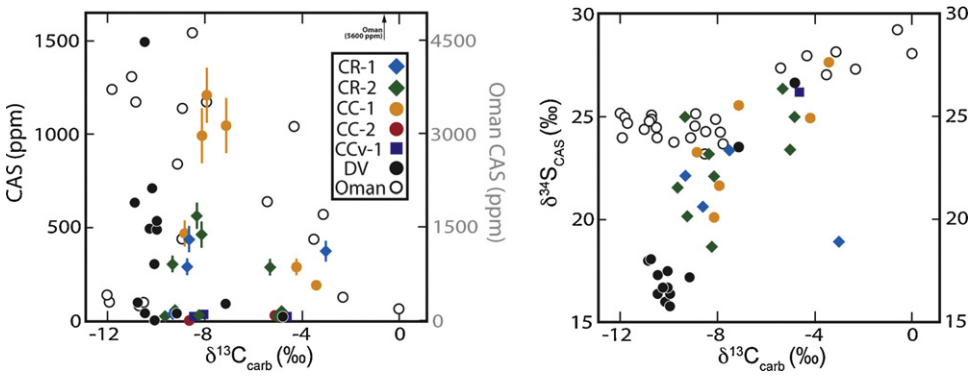

Fig. 12. Cross plot of CAS versus $\delta^{13}C_{carb}$ (left) and $\delta^{34}S_{CAS}$ versus $\delta^{13}C_{carb}$ (right) for the W–S inception and isotopic minimum facies from Sonora, Death Valley (from Kaufman et al., 2007) and Oman (from Fike et al., 2006). Notice good positive correlation between $\delta^{34}S_{CAS}$ and $\delta^{13}C_{carb}$. A looser correlation between CAS concentration and $\delta^{13}C_{carb}$ likely reflects the combined effects of a primary depositional signal and variable diagenetic removal of CAS in all data sets.

on sulfate incorporation and/or preservation in carbonate rocks. This is due to the fact that similar lithologies (i.e., oolites, finely laminated carbonates, etc.) within the sections but not associated with the marker beds record consistently low [CAS]. However, the incorporation of sulfate into the carbonate crystal lattice is still poorly understood and additional research must be conducted along these lines. Nevertheless, the increase in [CAS] observed here and elsewhere in contemporaneous units, along with coeval trends in isotope records, make an at least partial primary origin for these signals reasonable, as discussed below.

As with the marker beds in Sonora, an increase in CAS concentration of similar magnitude is observed in time-equivalent carbonates of the Rainstorm Member (Johnnie Formation) in the Death Valley region (Fig. 9; Kaufman et al., 2007). The Rainstorm carbonates also contain similar lithologic transitions (oolite lying stratigraphically below a finely laminated carbonate) and enigmatic fabrics (FPC and formerly aragonitic crystal fans; Corsetti and Kaufman, 2003; Pruss et al., 2008). The increased [CAS] in ~580 Ma carbonates from Death Valley and Sonora may reflect a transient increase in seawater sulfate. The spatial scale of this increase is difficult to constrain, and extrapolation to a global increase in marine sulfate is far from justifiable given the lack of [CAS] data from additional, more distant localities and the growing likelihood of a globally heterogeneous Neoproterozoic ocean (Hurtgen et al., 2006; Loyd et al., 2012; Lyons and Gill, 2008; Lyons et al., 2009, 2012). However, the [CAS] increases in Sonora and Death Valley carbonates do indicate some degree of continuity over ~800 km of lateral distance—or less, if one accepts the Sonora-Mojave megashear hypothesis, which suggests that Sonora and Death Valley were subsequently displaced from one another along a major, now obscured, fault zone (cf., Anderson and Silver, 2005; Stewart, 2005).

Sulfur isotope values for CAS from the Clemente marker bed show somewhat differing stratigraphic trends among the five sections studied (Figs. 7 and 9). Section CC-1 has a $\delta^{34}S_{CAS}$ trend similar to that of the Rainstorm Member carbonates of Death Valley, with isotope values decreasing ~7–10‰ near the middle to upper portions of the section (Kaufman et al., 2007). CR-2 also exhibits a mid-section decrease in $\delta^{34}S_{CAS}$; however, a less severe increase of ~3‰ occurs in the lower 60 cm of the marker bed. Finally, section CR-1 displays an overall increase in $\delta^{34}S_{CAS}$, with a mid-section maximum of ~23‰ (it is important to note that this is still lower than non-marker bed carbonates of the Clemente Formation of Cerro Rajón). The observed differences among the Clemente marker beds demonstrates very localized variability in $\delta^{34}S_{CAS}$. Hurtgen et al. (2006) also report significant variation in $\delta^{34}S_{CAS}$ among sections of the Namibian Maieberg cap carbonate (Marinoan) separated by ~200 km of lateral distance. However, these authors also noted good agreement in $\delta^{34}S_{CAS}$ among nearby sections of the same unit. The younger (~580 Ma) carbonates of the Clemente marker bed show significant variability (up to 9‰) over a mere ~25 km of lateral distance, suggestive of localized controls on seawater $\delta^{34}S_{sulfate}$.

Despite differences in the details, the five Sonora sections and the one Death Valley section record similar stratigraphic trends. While the Death Valley section exhibits a siliciclastic interval between the lower oolite and upper fan bearing carbonates (Corsetti and Kaufman, 2003), the Sonora sections all contain a basal oolite directly overlain by hummocky cross-stratified, fan-bearing, pink carbonate. Therefore, the Sonora carbonate marker beds represent equivalents deposited at essentially the same depth. The variation in $\delta^{34}S_{CAS}$ among the five sections indicates that lateral variability in $\delta^{34}S_{sulfate}$ (as opposed to vertical variability potentially arising from a stratified water column) could have existed at ~580 Ma, even across short lateral distances.

5.7. *The Clemente and Rainstorm W–S facies: a paleoenvironmental interpretation*

Despite noticeable variability in $\delta^{34}S_{CAS}$ among the Clemente marker bed sites, sections from Cerro Rajón exhibit sulfur isotope values that are up to ~8‰ depleted compared to carbonates stratigraphically below (~26‰) and above (~28‰) (see Fig. 5 in Loyd et al., 2012). These decreased isotopic values and an increase in [CAS] of ~1000 ppm in the most unaltered samples, suggest an increased input of isotopically light sulfate to local (perhaps regional) seawater. The ultimate extent of the sulfate increase is poorly constrained; however, given the broad similarities between the Clemente marker bed and the Rainstorm carbonates of Death Valley, ~800 km of Neoproterozoic shelf could have impacted. In addition, $\delta^{34}S_{CAS}$ and $\delta^{13}C_{carb}$ exhibit good positive correlation in both the Clemente and Rainstorm marker beds (Fig. 12) potentially indicative of a common source of sulfate and bicarbonate/carbonate.

The data presented here and those from Death Valley (Kaufman et al., 2007) can be explained by a transient oxygenation event (see Fig. 13). The transient oxygenation interpretation differs from others concerning the W–S anomaly, which generally involve a rapid global increase in pO_2 to near-modern levels that are more or less sustained through the remainder of Earth history (Canfield et al., 2007; Fike et al., 2006; McFadden et al., 2008; Rothman et al., 2003). Whereas the sulfur isotope trends differ significantly between pre- and post-W–S units in Oman (Fike et al., 2006), all of the other analyzed study sites exhibit post excursion trends (and/or variability)

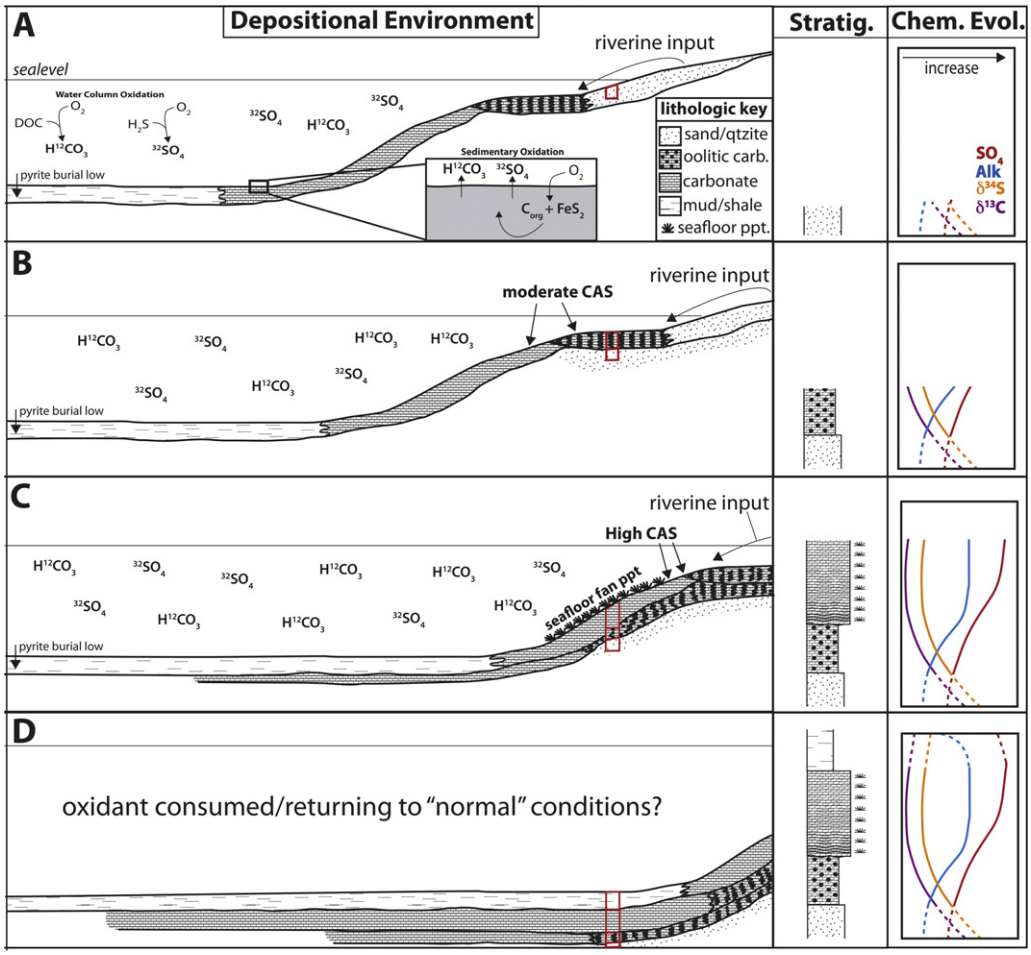

Fig. 13. Diagrammatic evolution of the Sonora region ~580 Ma. Time progresses alphabetically from A to D and the depositional environment, stratigraphic progression and chemical evolution are shown for each time slice. The stratigraphic progression from quartzite to oolite to laminated micrite to shale suggests a deepening depositional environment consistent with transgression. Flat-pebble facies are laterally discontinuous and not shown here. In this interpretative diagram, oxygenation is shown affecting water column and/or sedimentary reduced phases, however, delivery of recently oxidized species on land could also have been important. All processes would lead to the observed trends in $\delta^{13}C_{carb}$, $\delta^{34}S_{CAS}$ and CAS concentration. In addition, oxidation of significant amounts of organic carbon could increase alkalinity and promote precipitation of extensive syndepositional seafloor cements including ooid coatings and crystal fans. The return to more 'Neoproterozoic-like' geochemical signatures in units above the excursion facies likely reflects the potential consumption of the associated oxidants.

that are indistinguishable from those of the earlier Neoproterozoic (Kaufman et al., 2007; Loyd et al., 2012; McFadden et al., 2008). These characteristics imply differential behavior among basins, with most displaying trends consistent with a transient oxygenation event(s). The trends of Sonora and Death Valley are discussed in more detail below.

It is difficult to identify the particular oxidant(s) responsible for oxygenation; however potential possibilities include free oxygen, nitrate and/or metal oxides. Given the uncertainties associated with the distribution of reduced species prior to the onset of this event, it is impossible (with the present data) to distinguish whether oxidation affected reduced sulfides and carbon (probably organic matter) located in (1) marine sediments, (2) the water column (similar to the deep dissolved organic carbon reservoir of Rothman et al., 2003) and/or (3) exposed sediments on land (as proposed by Kaufman et al., 2007). Regardless of the exact initial location of reduced species, oxidants could react with sulfides and organic carbon and yield their respective oxidized counterparts SO_4^{2-} and HCO_3^-. Due to the isotopic nature of the reduced parent species, the resultant oxidized phases would also be isotopically depleted, as there is no significant fractionation associated with oxidation. In addition, the residual pyrite and organic carbon contents could be low in the sediments, particularly if the oxidant penetrated the sediment column and/or reacted with dissolved species in the water column, thereby limiting their delivery to the underlying sediments. Whereas organic carbon contents have not been determined in Sonora carbonates, pyrite contents are exceedingly low (Table 1), potentially indicative of shallow sedimentary and/or water column sulfide oxidation (sample insoluble contents of ~10–20% suggest that low iron availability probably did not limit pyrite formation). Additionally, organic carbon contents from the Death Valley W–S interval are relatively low and show a sharp decrease in the Johnnie Oolite (Kaufman et al., 2007), which lends further support to the oxidation hypothesis. Although, it should be noted that the controls on organic carbon contents are complex and low concentrations may have been brought on for unrelated reasons, particularly in rocks of such antiquity.

Finally, given sufficient Ca^{2+}, an oxidation-produced increase in HCO_3^- (or CO_3^{2-}) would promote conditions more favorable for carbonate precipitation and could have led to the development of extensive oolite deposition and aragonite seafloor fan precipitation. In fact, simple mass balance dictates that the decrease in $\delta^{13}C_{carb}$ of ~10‰ (down to ~−10‰) would require a nearly two-fold increase in the marine dissolved inorganic carbon reservoir, provided that organic carbon with an isotopic composition of ~−25‰ was the primary oxidized substrate (and an initial marine $\delta^{13}C$ of ~0‰). Such

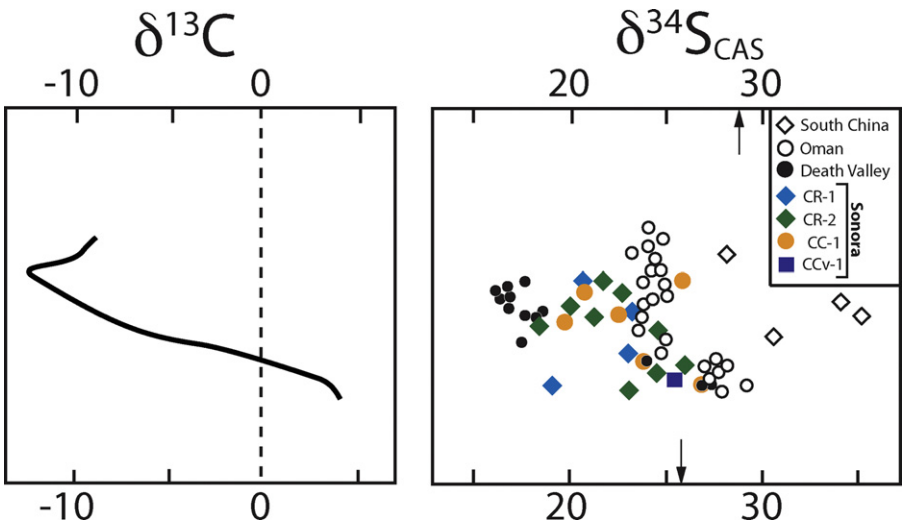

Fig. 14. Global comparison of $\delta^{34}S_{CAS}$ data using correlation via $\delta^{13}C_{carb}$. A general, up-section trend toward lower $\delta^{34}S_{CAS}$ values occurs in W–S equivalent facies from Sonora, Death Valley and Oman, however at each locality the absolute values differ. The data from S. China do not exhibit a decreasing trend in $\delta^{34}S_{CAS}$ in the excursion inception and nadir facies. The arrows correspond to the $\delta^{34}S_{CAS}$ values of underlying and overlying carbonates from Cerro Rajón (Loyd et al., 2012). Death Valley data from Kaufman et al. (2007), Oman data from Fike et al. (2006), S. China data from McFadden et al. (2008).

a vast input of dissolved inorganic carbon could have prompted widespread and rapid carbonate precipitation, although limits on the spatial extent of carbonate precipitation are difficult to constrain at this point.

In order to attribute all of these trends to a transient oxygenation event, specific initial conditions for the Sonora and Death Valley regions are required. In order to develop local perturbations in $\delta^{34}S_{sulfate}$, the initial sulfate reservoir must have been low (perhaps <~2 mM, Loyd et al., 2012), a condition supported by the relatively low concentrations of CAS, highly variable $\delta^{34}S_{CAS}$ and $\delta^{34}S_{pyr}$ (Hurtgen et al., 2005; Loyd et al., 2012; McFadden et al., 2008), heterogeneous $\delta^{34}S_{CAS}$ (Hurtgen et al., 2006; Loyd et al., 2012; Lyons et al., 2009, 2012) and low or even negative $\Delta^{34}S_{CAS\text{-}pyr}$ (Ries et al., 2009; Shen et al., 2008, 2010, 2011) in non-W–S Neoproterozoic carbonates. In addition, low sulfate concentrations must have existed prior to and after the oxygenation event by continuous removal via BSR in order to account for a significant decrease in $\delta^{34}S_{sulfate}$ (such as the ~8‰ drop observed here) upon sulfide oxidation (recall that isotopically light pyrite is primarily generated as a byproduct of BSR).

When combined, the data suggest that Death Valley and Sonora experienced similar depositional conditions at ~580 Ma. Both locations were either part of one continuous depositional system or perhaps individual, isolated basins encountering similar processes. Similar depositional conditions are geologically reasonable, given that the much of the western edge of North America was experiencing a similar tectonic transition (from a rifted to a passive margin, Levy et al., 1994). The local deviation in $\delta^{34}S_{CAS}$ in the Clemente marker bed and Rainstorm carbonates can be explained by differences in the degree of oxidation and by local deviations in $\delta^{34}S_{pyr}$. Variations in CAS concentrations may likewise reflect differences in the quantity of sulfide oxidized, differences in diagenetic removal and/or complexities associated with sulfate incorporation into the carbonate lattice (e.g., Busenberg and Plummer, 1985). Strong correlation with Fe_{carb} would suggest at least some influence by diagenetic removal, as discussed above, such that those samples with the highest [CAS] are likely most reflective of the primary environment. Ultimately, the increased CAS concentration, reduced and correlated sulfur and carbon isotopic compositions, absence of pyrite and presence of various high alkalinity indicators can all be explained by a transient oxygenation event ~580 million years ago. Better age constraints and additional spatial characterization are necessary to further understand the duration and extent of this potential event. At this stage it is unclear how an oxidation event would specifically perturb the ancient Death Valley and Sonora marine systems. Future modeling efforts that couple carbon and sulfur isotope behavior will be instrumental in helping better constrain system inputs and outputs and potentially allow for the quantification of system response times. Here, we argue that the data as a whole are consistent with an oxidation event and therefore provide an associated testable hypothesis.

5.8. Broad implications: global heterogeneity in $\delta^{34}S_{sulfate}$

Using the W–S excursion as a global tie point, $\delta^{34}S_{CAS}$ records from Oman, South China, Death Valley and Sonora can be directly compared (Fig. 14). The compilation demonstrates that similar to Sonora and Death Valley, the inception and isotopic minimum of the W–S in Oman exhibit decreasing $\delta^{34}S_{CAS}$ values and drastically increasing CAS concentrations (Fike et al., 2006). In contrast, the same interval from S. China exhibits a unique trend (McFadden et al., 2008). Although the general characteristics of $\delta^{34}S_{CAS}$ are similar among most of the excursion facies (Sonora, Death Valley and Oman, see Fig. 14), the lack of agreement in the absolute values of $\delta^{34}S_{CAS}$ beyond anything we can easily attribute to diagenesis suggests that the marine realm was heterogeneous with respect to $\delta^{34}S_{sulfate}$ during this time interval. Similar heterogeneity in $\delta^{34}S_{CAS}$ is recorded in coeval, Cambrian-aged rocks from multiple localities, interpreted by Gill et al. (2011) and Loyd et al. (2012) as evidence for sustained low sulfate conditions. The heterogeneity in $\delta^{34}S_{CAS}$ suggests that models and reconstructions based on singular, inferred global $\delta^{34}S_{sulfate}$ values are somewhat flawed and inconsistent with the observed intra-basinal variations. In addition, it is evident that $\delta^{34}S_{CAS}$ alone cannot be used as a chemostratigraphic correlation tool in Neoproterozoic carbonates even if the signal is interpreted as primary.

The global expression of the W–S excursion remains somewhat perplexing. If attributed to an oxygenation event in the Clemente and Rainstorm carbonates, then are similar interpretations warranted elsewhere? Indeed many hypotheses are centered on oxygenation of at least some portions of the ocean-atmosphere system, a particularly attractive hypothesis given the coincident evolution of macroscopic life (Johnston et al., 2012; Knoll, 1996). However, the precise nature of oxygenation and the sources of the

parent reduced carbon species are highly debated (Canfield et al., 2007; Fike et al., 2006; Kaufman et al., 2007; McFadden et al., 2008; Rothman et al., 2003), as well as the possibility of a diagenetic origin (Bristow and Kennedy, 2008; Derry, 2010; Grotzinger et al., 2011; Knauth and Kennedy, 2009; Swart and Kennedy, 2012). If the W–S is indeed a primary signal, we argue that no singular process needs to account for the global oceans and stress that an input of oxidants are likely to affect many if not all reduced reservoirs to varying degrees. For this reason, alternate basins may exhibit similar carbon isotope but unique (and perhaps delayed as in S. China, McFadden et al., 2008) sulfur isotope behavior and still record an oxygenation event. Indeed, the post-W–S transition to low stratigraphic variability in $\delta^{34}S_{CAS}$ in Oman contrasts significantly with the successions of Sonora and Death Valley, which both exhibit post W–S variability of the same magnitude as prior to the excursion (Loyd et al., 2012). It seems that during the W–S interval, multiple (but not all) basins record similar $\delta^{34}S_{CAS}$ trends, potentially indicative of an oxygenation-associated increased sulfate reservoir. However, the geochemical differences in post-excursion facies suggest that the sulfate increase was transient in some basins and possibly more long-lived in others, reflecting differences in how each basin responds to an input of oxidants. Such local behavior may relieve the requirement of extreme oxidant draw down as a result of whole ocean oxygenation as has been proposed as evidence against a primary W–S origin (Bristow and Kennedy, 2008). As mentioned above, additional geochemical modeling will help resolve these issues. Regardless of the particular controls of the sulfur isotopic composition of marine sulfate, the hypothesis of a heterogeneous $\delta^{34}S_{sulfate}$ Neoproterozoic ocean seems to continuously gain support.

6. Conclusions

A locally extensive, carbonate marker bed of the Clemente Formation, Sonora, Mexico expresses $\delta^{13}C_{carb}$ values down to ~−10‰, consistent with the globally expressed Wonoka–Shuram (W–S) isotope excursion. This marker bed exhibits high variability in CAS concentration and moderate variability in $\delta^{34}S_{CAS}$ over ~25 km of lateral distance. Negative correlation of CAS concentration with Mn/Sr ratios and Fe_{carb} concentrations in all samples is consistent with removal of CAS during diagenetic recrystallization, and samples exhibiting high [CAS] are likely most reflective of the most primary values. $\delta^{34}S_{CAS}$ does not show correlation with these traditional proxies for diagenesis, suggesting an alternate source of variability, probably arising from local variations in seawater $\delta^{34}S_{sulfate}$.

As a whole, marker bed sulfur systematics are similar to those from coeval fan-bearing carbonates of the Johnnie Formation, Death Valley, California. Both sites show an increase in CAS concentration and a decrease in $\delta^{34}S_{CAS}$ and $\delta^{13}C_{carb}$ compared to overlying and underlying carbonates. These trends, in addition to decreased pyrite and the presence of extensive seafloor precipitates, are consistent with a transient oxygenation event.

The W–S excursion has been recognized in many basins worldwide, and sulfur isotope profiles have been developed from two additional localities in Oman and S. China. Whereas similar trends in $\delta^{34}S_{CAS}$ and CAS concentration are recognized in some temporally equivalent units, the absolute values of $\delta^{34}S_{CAS}$ differ, suggesting that: (1) the Neoproterozoic oceans were not globally homogeneous with respect to $\delta^{34}S_{sulfate}$ and (2) if the trends represent an oxygenation event, each particular basin reacted somewhat differently. This study highlights the likelihood of global heterogeneity in Neoproterozoic $\delta^{34}S_{CAS}$, which must be considered in order to characterize oceanic $\delta^{34}S_{sulfate}$, and demonstrates that, unlike $\delta^{13}C_{carb}$, $\delta^{34}S_{CAS}$ cannot be used as a correlation tool by itself.

Acknowledgments

We would like to thank Steven Bates, Will Berelson, Dave Bottjer, Doug Hammond, Stew Hollingsworth, Katherine Marenco, Victoria Petryshyn, Miguel Rincon, Jack Stewart and Lowell Stott. David Fike provided a constructive and insightful review. SJL is currently supported by the Agouron Postdoctoral Fellowship Fund. Funding was provided to AJK, SJL and FAC by NSF and TWL by the NASA Exobiology Program. Additional funding was provided to SJL by the Lewis and Clark Fund (American Philosophical Society).

References

Allan, J.R., Mathews, R.K., 1982. Isotope signatures associated with early meteoric diagenesis. Sedimentology 29, 797–817.
Amthor, J.E., Grotzinger, J.P., Schroeder, S., Bowring, S., Ramezani, J., Martin, M.W., Matter, A., 2003. Extinction of *Cloudina* and *Namacalathus* at the Precambrian–Cambrian boundary in Oman. Geology 31, 431–434.
Anderson, T.H., J. Ealls, L. T. Silver, 1979. Geology of the Precambrian and Paleozoic rocks, Caborca-Bamori region. In: Anderson, T.H., Roldan-Quintana, J. (Eds.), Geology of northern Sonora. Pittsburgh, Pennsylvania, and Hermosillo, Mexico, University of Pittsburgh and Instituto de Geologia, Guidebook for fieldtrip 27, Geological Society of America Annual Meeting, 1–22.
Anderson, T.H., Silver, L.T., 2005. The Mojave-Sonora megashear—field and analytical studies leading to the conception and evolution of the hypothesis. In: Anderson, T.H., Nourse, J.A., McKee, J.W., Steiner, M.B. (Eds.), The Mojave-Sonora Megashear Hypothesis: Development, Assessment, and Alternatives. Geological Society of America Special Paper 393, pp. 1–50.
Banner, J.L., Hanson, G.N., 1990. Calculation of simultaneous isotopic and trace element variations during water-rock interaction with applications to carbonate diagenesis. Geochimica et Cosmochimica Acta 54, 3123–3137.
Bathurst, R.G.C., 1975. Carbonate Sediments and their Diagenesis, 2nd ed. Elsevier, Amsterdam, p. 620.
Bodine, M.W., Holland, H.D., Borcsik, M., 1965. Coprecipitation of manganese and strontium with calcite. In: Symposium of Problems of Postmagmatic Ore Deposition, 11, Prague, pp. 401–406.
Bowring, S.A., Myrow, P.M., Landing, E., Ramezani, J., 2002. Geochronological constraints on terminal Neoproterozoic events and the rise of Metazoans. Astrobiology 2, 112.
Bowring, S.A., Grotzinger, J.P., Condon, D.J., Ramezani, J., Newall, M.J., Allen, P.A., 2007. Geochronological constraints on the chronostratigraphic framework of the Neoproterozoic Huqf Supergroup. Sultanate of Oman: American Journal of Science 307, 1097–1145.
Brand, U., Veizer, J., 1980. Chemical diagenesis of a multicomponent carbonate system—1: trace elements. Journal of Sedimentary Petrology 50, 1219–1236.
Bristow, T.F., Kennedy, M.J., 2008. Carbon isotope excursions and the oxidant budget of the Ediacaran atmosphere and ocean. Geology 36, 863–866.
Burdett, J.W., Arthur, M.A., Richardson, M., 1989. A Neogene seawater sulfur isotope age curve from calcareous pelagic microfossils. Earth and Planetary Science Letters 94, 189–198.
Burns, S.J., Matter, A., 1993. Carbon isotopic record of the latest Proterozoic from Oman. Eclogae Geologicae Helvetiae 86, 595–607.
Burns, S.J., Haudenschild, U., Matter, A., 1994. The strontium isotopic composition of carbonates from the late Precambrian (ca. 560–540) Huqf Group of Oman. Chemical Geology 111, 269–282.
Busenberg, E., Plummer, L.N., 1985. Kinetic and thermodynamic factors controlling the distribution of SO_4^{2-} and Na^+ in calcites and selected aragonites. Geochimica et Cosmochimica Acta 49, 713–725.
Calver, C.R., 2000. Isotope stratigraphy of the Ediacaran (Neoproterozoic III) of the Adelaide Rift Complex, Australia, and the overprint of water column stratification. Precambrian Research 100, 121–150.
Canfield, D.E., Raiswell, R., Westrich, J.T., Reaves, C.M., Berner, R.A., 1986. The use of chromium reduction in the analysis of reduced inorganic sulfur in sediments and shales. Chemical Geology 54, 149–155.
Canfield, D.E., Poulton, S.W., Narbonne, G.M., 2007. Late-Neoproterozoic deep-ocean oxygenation and the rise of animal life. Science 315, 92–95.
Condon, D., Zhu, M., Bowring, S., Wang, W., Yang, A., Jin, Y., 2005. U–Pb ages from the Neoproterozoic Doushantuo Formation, China. Science 308, 95–98.
Corsetti, F.A., Kidder, D.L., Marenco, P.J., 2006. Trends in dolomitization across the Neoproterozoic–Cambrian boundary: a case study from Death Valley, California. Sedimentary Geology 191, 135–150.
Corsetti, F.A., Hagadorn, J.W., 2000. Precambrian–Cambrian transition: Death Valley, United States. Geology 28, 299–302.
Corsetti, F.A., Kaufman, A.J., 2003. Stratigraphic investigations of carbon isotope anomalies and Neoproterozoic ice ages in Death Valley, California. Geological Society of America Bulletin 115, 916–932.
Damon, P.E., Livingston, D.E., Mauger, R.L., Giletti, B.J., Pantoja-Alor, J., 1962. Edad de Precambrico Anterior y de otras rocas del zócalo de la region de Caborca-Altar de la parte noroccidental del Estado Sonora, vol. 64. Universidad Nacional Autónoma de México, Instituto de Geologia Boletin, pp. 11–44.
Derry, L.A., 2010. A burial diagenesis origin for the Ediacaran Wonoka–Shuram carbon isotope anomaly. Earth and Planetary Science Letters 294, 152–162.

Fike, D.A., Grotzinger, J.P., Pratt, L.M., Summons, R.E., 2006. Oxidation of the Ediacaran ocean. Nature 444, 744–747.
Fike, D.A., Grotzinger, J.P., 2008. A paired sulfate–pyrite $\delta^{34}S$ approach to understanding the evolution of the Ediacaran–Cambrian sulfur cycle. Geochimica et Cosmochimica Acta 72, 2636–2648.
Folk, R.L., 1965. Some aspects of recrystallization in ancient limestones. In: Pray, L.C., Murray, R.C. (Eds.), Dolomitization and Limestone Diagenesis: A Symposium. Soc. Econ. Paleontologists Mineralogists Special Publication 13, pp. 14–48.
Gill, B.C., Lyons, T.W., Frank, T.D., 2008. Behavior of carbonate-associated sulfate during meteoric diagenesis and implications for the sulfur isotope paleoproxy. Geochimica et Cosmochimica Acta 72, 4699–4711.
Gill, B.C., Lyons, T.W., Young, S.A., Kump, L.R., Knoll, A.H., Saltzman, M.R., 2011. Geochemical evidence for widespread euxinia in the Later Cambrian ocean. Nature 469, 80–83.
Gomez Peral, L.E., Poire, D.G., Strauss, H., Zimmermann, U., 2007. Chemostratigraphy and diagenetic constraints on Neoproterozoic carbonate successions from the Sierras Bayas Group, Tandilia System, Argentina. Chemical Geology 237, 127–146.
Grotzinger, J.P., Bowring, S.A., Saylor, B.Z., Kaufman, A.J., 1995. Biostratigraphic and geochronologic constraints on early animal evolution. Science 270, 598–604.
Grotzinger, J.P., Fike, D.A., Fisher, W.W., 2011. Enigmatic origin of the largest-known carbon isotope excursion in Earth's history. Nature Geoscience 4, 285–292.
Halverson, G.P., Hoffman, P.F., Schrag, D.P., Maloof, A.C., Rice, A.H.N., 2005. Toward a Neoproterozoic composite carbon-isotope record. Geological Society of America Bulletin 117, 1181–1207.
Halverson, G.P., Hurtgen, M.T., 2007. Ediacaran growth of the marine sulfate reservoir. Earth and Planetary Science Letters 263, 32–44.
Halverson, G.P., Wade, B.P., Hurtgen, M.T., Barovich, K.M., 2012. Neoptroterozoic chemostratigraphy. Precambrian Research 182, 337–350.
Hurtgen, M.T., Arthur, M.A., Prave, A.R., 2004. The sulfur isotopic composition of carbonate associated sulfate in Mesoproterozoic to Neoproterozoic carbonates from Death Valley, California. In: Amend, J., Edwards, K., Lyons, T.W. (Eds.), Microbial Sulfur Transformations Throughout Earth's History: Development, Changes, and Future of the Biogeochemical Sulfur Cycle. Geological Society of America Special Paper 379, Boulder, CO, pp. 177–194.
Hurtgen, M.T., Arthur, M.A., Halverson, G.P., 2005. Neoproterozoic sulfur isotopes, the evolution of microbial sulfur species, and the burial efficiency of sulfide as sedimentary pyrite. Geology 33, 41–44.
Hurtgen, M., Halverson, G., Arthur, M., Hoffman, P., 2006. Sulfur cycling in the aftermath of a Neoproterozoic (Marinoan) snowball glaciation: evidence for a syn-glacial sulfidic deep ocean. Earth and Planetary Science Letters 245, 551–570.
Hurtgen, M.T., Pruss, S.B., Knoll, A.H., 2009. Evaluating the relationship between the carbon and sulfur cycles in the later Cambrian ocean: an example from the Port au Port Group, western Newfoundland, Canada. Earth and Planetary Science Letters 281, 288–297.
Jiang, G., Kaufman, A.J., Christie-Blick, N., Zhang, S., Wu, H., 2007. Carbon isotope variability across the Ediacaran Yangtze platform in South China: implications for a large surface-to-deep ocean $\delta^{13}C$ gradient. Earth and Planetary Science Letters 261, 303–320.
Johnston, D.T., Poulton, S.W., Goldberg, T., Sergeev, V.N., Podkovyrov, V., Vorob'eva, N.G., 2012. Late Ediacaran redox stability and metazoan evolution. Earth and Planetary Science Letters 335–336, 25–35.
Kaufman, A.J., Jiang, G., Christie-Blick, N., Banergee, D.M., Rai, V., 2006. Stable isotopic record of the terminal Neoproterozoic Krol platform in the Lesser Himalayas of northern India. Precambrian Research 147, 156–185.
Kaufman, A.J., Corsetti, F.A., Varni, M.A., 2007. The effect of rising atmospheric oxygen on carbon and sulfur isotope anomalies in the Neoproterozoic Johnnie Formation, Death Valley, USA. Chemical Geology 237, 65–81.
Kinsman, D.J., 1969. Interpretation of Sr^{2+} concentrations in carbonate minerals and rocks. Journal of Sedimentary Petrology 39, 486–508.
Knauth, L.P., Kennedy, M.J., 2009. The late Precambrian greening of the Earth. Nature 460, 728–732.
Knoll, A.H., 1996. Breathing room for early animals. Nature 382, 111–112.
Le Guerroue, E., Allen, P.A., Cozzi, A., Etienne, J.L., Fanning, M., 2006a. 50 million year duration negative carbon isotope excursion in the Ediacaran ocean. Terra Nova 18, 147–153.
Le Guerroue, E., Allen, P.A., Cozzi, A., 2006b. Chemostratigraphic and sedimentological framework of the largest negative carbon isotopic excursion in Earth history: the Neoproterozoic Shuram Formation (Nafun Group, Oman). Precambrian Research 146, 68–92.
Levy, M., Christie-Blick, N., Link, P.K., 1994. Neoproterozoic incised valleys of the eastern Great Basin, Utah and Idaho: fluvial response to changes in depositional base level. In: Dalrymple, R.W., Boyd, R., Zaitlin, B.A. (Eds.), Incised-Valley Systems: Origin and Sedimentary Sequences. SEPM Special Publication 51, pp. 369–382.
Li, C., Love, G.D., Lyons, T.W., Fike, D.A., Sessions, A.L., Chu, X., 2010. A stratified redox model for the Ediacaran ocean. Science 328, 80–83.
Loyd, S.J., Marenco, P.J., Hagadorn, J.W., Lyons, T.W., Kaufman, A.J., Sour-Tovar, F., Corsetti, F.A., 2012. Sustained low marine sulfate concentrations from the Neoproterozoic to the Cambrian: insights from carbonates of northwestern Mexico and eastern California. Earth and Planetary Science Letters 339–340, 79–94.
Lyons, T.W., Gill, B.C., 2008. Ancient sulfur cycling and oxygenation of the early biosphere. Elements 6, 93–99.
Lyons, T.W., Walter, L.M., Gellatly, A.M., Marini, A.M., Blake, R.E., 2004. Sites of anomalous organic remineralization in the carbonate sediments of South Florida, U.S.A.: the sulfur cycle and carbonate-associated sulfate. In: Amend, J., Edwards, K., Lyons, T.W. (Eds.), Microbial Sulfur Transformations Throughout Earth's History: Development, Changes, and Future of the Biogeochemical Sulfur Cycle. Geological Society of America Special Paper 379, Boulder, CO, pp. 161–176.
Lyons, T.W., Anbar, A.D., Severmann, S., Scott, C., Gill, B.C., 2009. Tracking euxinia in the ancient ocean: a multiproxy perspective and Proterozoic case study. Annual Reviews in Earth and Planetary Sciences 37, 507–534.
Lyons, T.W., Reinhard, C.T., Love, G., Xiao, S., 2012. Geobiology of the Proterozoic Eon. In: Canfield, D.E., Knoll, A.H., Konhauser, K. (Eds.), Fundamentals in Geobiology. John Wiley & Sons Ltd., Chichester, UK (Chapter 20).
Mazumdar, A., Goldberg, T., Strauss, H., 2008. Abiotic oxidation of pyrite by Fe(III) in acidic media and its implications for sulfur isotope measurements of lattice-bound sulfate in sediments. Chemical Geology 253, 30–37.
Macdonald, F.A., Jones, D.S., Schrag, D.P., 2009. Stratigraphic and tectonic implications of a newly discovered glacial diamictite-cap carbonate couplet in southwestern Mongolia. Geology 37, 123–126.
Marenco, P.J., Corsetti, F.A., Hammond, D.E., Kaufman, A.J., Bottjer, D.J., 2008. Oxidation of pyrite during extraction of carbonate associated sulfate. Chemical Geology 247, 124–132.
McFadden, K.A., Huang, J., Chu, X., Jiang, G., Kaufman, A.J., Zhou, C., Yuan, X., Xiao, S., 2008. Pulsed oxidation and biological evolution in the Ediacaran Doushantuo Formation. Proceedings of the National Academy of Science 105, 3197–3202.
McMenamin, M.A.S., 1984. Paleontology and stratigraphy of Lower Cambrian and Upper Proterozoic sediments, Caborca region, northwestern Sonora, Mexico. Unpublished Ph.D. Thesis, University of California, Santa Barbara, CA, 218 pp.
McMenamin, M.A.S., 1996. Ediacaran biota from Sonora, Mexico. Proceedings of the National Academy of Sciences 93, 4990–4993.
Nascimento, R.S.C., Sial, A.N., Pimentel, M.M., 2007. C- and Sr-isotope systematics applied to Neoproterozoic marbles of the Serido belt, northeastern Brazil. Chemical Geology 237, 209–228.
Nogueira, A.C.R., Riccomini, C., Sial, A.N., Moura, C.A.V., Trindale, R.I.F., Fairchild, T.R., 2007. Carbon and strontium isotope fluctuations and paleoceanographic changes in the late Neoproterozoic Araras carbonate platform, southern Amazon craton, Brazil. Chemical Geology 237, 186–208.
Prave, A.R., Fallick, A.E., Thomas, C.W., Graham, C.M.A., 2009. A composite C-isotope profile for the Neoproterozoic Dalradian Supergroup of Scotland and Ireland. Journal of the Geological Society 166, 845–857.
Pruss, S.B., Corsetti, F.A., Fischer, W.W., 2008. Seafloor-precipitated carbonate fans in the Neoproterozoic Rainstorm Member, Johnnie Formation, Death Valley Region, USA. Sedimentary Geology 207, 34–40.
Ries, J.B., Fike, D.A., Pratt, L.M., Lyons, T.W., Grotzinger, J.P., 2009. Superheavy pyrite (δ34Spyr > δ34SCAS) in the terminal Proterozoic Nama Group, southern Namibia: A consequence of low seawater sulfate at the dawn of animal life. Geology 37, 743–746.
Rodríguez-Castañeda, J.L., 1994. Geologia del área el Teguachi, Estado de Sonora, Mexico. Revista Mexicana de Ciencias Geologicas 11, 11–28.
Rothman, D.H., Hayes, J.M., Summons, R.E., 2003. Dynamics of the Neoproterozoic carbon cycle. Proceedings of the National Academy of Sciences 100, 8124–8129.
Sandberg, P.A., 1975. New interpretations of Great Salt Lake ooids and of ancient non-skeletal carbonate mineralogy. Sedimentology 22, 497–537.
Shen, B., Xiao, S., Kaufman, A.J., Bao, H., Zhou, C., Wang, H., 2008. Stratification and mixing of a post-glacial Neoproterozoic ocean: Evidence from carbon and sulfur isotopes in a cap dolostones from northwest China. Earth and Planetary Science Letters 265, 209–228.
Shen, B., Xiao, S., Zhou, C., Kaufman, A.J., Yuan, X., 2010. Carbon and sulfur isotope chemostratigraphy of the Neoproterozoic Quanji Group of the Chaidam Basin, NW China: Basin stratification in the aftermath of an Ediacaran glaciation postdating the Shuram event? Precambrian Research 177, 241–251.
Shen, B., Xiao, S., Bao, H., Kaufman, A.J., Zhou, C., Yuan, X., 2011. Carbon, sulfur, and oxygen isotope evidence for a strong depth gradient and oceanic oxidation after the Ediacaran Hankalchough glaciation. Geochimica et Cosmochimica Acta 75, 1357–1373.
Sibley, D.F., 1991. Secular changes in the amount and texture of dolomite. Geology 19, 151–154.
Sour-Tovar, F., Hagadorn, J.W., Huitron-Rubio, T., 2007. Ediacaran and Cambrian index fossils from Sonora, Mexico. Palaeontology 50, 169–175.
Sperling, E.A., Pisani, D., Peterson, K.J., 2007. Poriferan paraphyly and its implications for Precambrian palaeobiology. In: Vickers-Rich, P., Komarower, P. (Eds.), The Rise and Fall of the Ediacaran Biota. Geological Society of America Special Publications 286, pp. 355–368.
Stewart, J.H., McMenamin, M.A.S., Morales-Ramirez, J.M., 1984. Upper Proterozoic and Cambrian rocks on the Caborca region, Sonora, Mexico—Physical stratigraphy, biostratigraphy, paleocurrent studies, and regional relations. USGS Professional Paper 309, 36 [p.
Stewart, J.H., 2005. Evidence for Mojave-Sonora megashear—Systematic left-lateral offset of Neoproterozoic to Lower Jurassic strata and facies, western United States and northwestern Mexico. In: Anderson, T.H., Nourse, J.A., McKee, J.W., Steiner, M.B. (Eds.), The Mojave-Sonora Megashear Hypothesis: Development, Assessment, and Alternatives. Geological Society of America Special Paper 393, pp. 209–231.
Swart, P.K., Kennedy, M.J., 2012. Does the global stratigraphic reproducibility of $\delta^{13}C$ in Neoproterozoic carbonates require a marine origin? A Pliocene-Pleistocene comparison. Geology 40, 87–90.

Tucker, M.E., 1983. Diagenesis, geochemistry, and origin of a Precambrian dolomite: the Beck Spring Dolomite of eastern California. Journal of Sedimentary Petrology 53, 1097–1119.
Tucker, M.E., Wright, V.P., 1990. Carbonate Sedimentology. Blackwell, Oxford, 482 pp.
Turekian, K.K., 1972. Chemistry of the Earth. Holt, Reinhart and Winston, New York, 131 pp.
Xiao, S., McFadden, K.A., Peek, S., Kaufman, A.J., Zhou, C., Jiang, G., Hu, J., 2012. Integrated chemostratigraphy of the Doushantuo Formation at the northern Xiaofenghe section (Yangtze Gorges, South China) and its implication for Ediacaran stratigraphic correlation and ocean redox models. Precambrian Research 192–195, 125–141.
Zempolich, W.G., Baker, P.A., 1993. Experimental and natural mimetic dolomitization of aragonite ooids. Journal of Sedimentary Petrology 63, 596–606.
Zhou, C., Xiao, S., 2007. Ediacaran $\delta^{13}C$ chemostratigraphy of South China. Chemical Geology 237, 65–81.